AD-A122 232 AN ALGEBRAIC TURBULENCE MODEL MODIFIED FOR EXTRA RATES OF STRAIN IN AN AX.. (U) PENNSYLVANIA STATE UNIV UNIVERSITY PARK APPLIED RESEARCH LAB.. G H HOFFMAN

UNCLASSIFIED 30 SEP 82 ARL/PSU/TM-82-201 F/G 20/4 NL

1/1

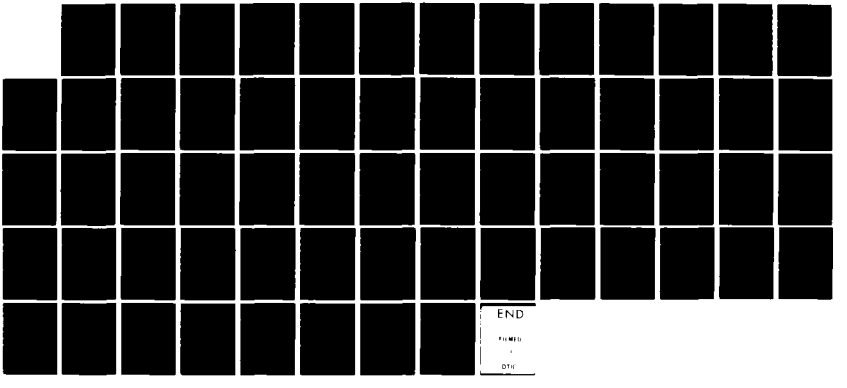

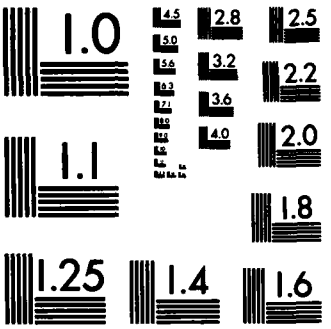

(6)

AN ALGEBRAIC TURBULENCE MODEL MODIFIED FOR EXTRA RATES OF STRAIN IN AN AXISYMMETRIC BOUNDARY LAYER

G. H. Hoffman

Technical Memorandum
File No. 82-201
30 September 1982
Contract No. N00024-79-C-6043

Copy No. 8

The Pennsylvania State University
Applied Research Laboratory
Post Office Box 30
State College, PA 16801

NAVY DEPARTMENT

NAVAL SEA SYSTEMS COMMAND

SECURITY CLASSIFICATION OF THIS PAGE *(When Data Entered)*

REPORT DOCUMENTATION PAGE		READ INSTRUCTIONS BEFORE COMPLETING FORM
1. REPORT NUMBER 82-201	2. GOVT ACCESSION NO. AD A122232	3. RECIPIENT'S CATALOG NUMBER
4. TITLE *(and Subtitle)* AN ALGEBRAIC TURBULENCE MODEL MODIFIED FOR EXTRA RATES OF STRAIN IN AN AXISYMMETRIC BOUNDARY LAYER		5. TYPE OF REPORT & PERIOD COVERED Technical Memorandum 6. PERFORMING ORG. REPORT NUMBER
7. AUTHOR*(s)* G. H. Hoffman		8. CONTRACT OR GRANT NUMBER*(s)* N00024-79-C-6043
9. PERFORMING ORGANIZATION NAME AND ADDRESS Applied Research Laboratory Post Office Box 30 State College, PA 16801		10. PROGRAM ELEMENT, PROJECT, TASK AREA & WORK UNIT NUMBERS
11. CONTROLLING OFFICE NAME AND ADDRESS Naval Sea Systems Command Washington, DC 20362 Code NSEA-63R31		12. REPORT DATE 30 September 1982 13. NUMBER OF PAGES 62
14. MONITORING AGENCY NAME & ADDRESS*(if different from Controlling Office)*		15. SECURITY CLASS. *(of this report)* UNCLASSIFIED 15a. DECLASSIFICATION/DOWNGRADING SCHEDULE

16. DISTRIBUTION STATEMENT *(of this Report)*

Approved for public release. Distribution unlimited per NAVSEA - November 26, 1982.

17. DISTRIBUTION STATEMENT *(of the abstract entered in Block 20, if different from Report)*

18. SUPPLEMENTARY NOTES

19. KEY WORDS *(Continue on reverse side if necessary and identify by block number)*

algebraic, turbulence, model, axisymmetric, boundary layer

20. ABSTRACT *(Continue on reverse side if necessary and identify by block number)*

A standard two-piece algebraic turbulence model is modified to account for transverse and longitudinal extra rates of strain which are important in the tail region of an axisymmetric boundary layer. The modified model contains one empirical constant which is determined with the aid of experimental data. For three bodies of revolution having different longitudinal curvature histories, boundary layer solutions with the modified and unmodified models are compared with detailed measurements. Incorporation of the two extra rates of strain is found to considerably improve agreement with the data in the tail region.

DD FORM 1 JAN 73 1473 EDITION OF 1 NOV 65 IS OBSOLETE

SECURITY CLASSIFICATION OF THIS PAGE *(When Data Entered)*

Subject: An Algebraic Turbulence Model Modified for Extra Rates of Strain in an Axisymmetric Boundary Layer

References: See page 25.

Abstract: A standard two-piece algebraic turbulence model is modified to account for transverse and longitudinal extra rates of strain which are important in the tail region of an asymmetric boundary layer. The modified model contains one empirical constant which is determined with the aid of experimental data. For three bodies of revolution having different longitudinal curvature histories, boundary layer solutions with the modified and unmodified models are compared with detailed measurements. Incorporation of the two extra rates of strain is found to considerably improve agreement with the data in the tail region.

Acknowledgement: This work was sponsored by the Naval Sea Systems Command, Code NSEA-63R1.

Table of Contents

Nomenclature

c_{fe}	wall friction coefficient = $\tau_w^*/\frac{1}{2}\rho^* u_e^{*2}$
H	axisymmetric shape factor = Δ^*/Θ
ℓ	mixing length
ℓ^+	mixing length in law-of-the-wall form = $\ell^* u_\tau^*/\nu^*$
L^*	body length (dimensional)
p	static pressure
P^+	pressure gradient parameter = $\nu^* \frac{dp^*}{dx^*}/\rho^* u_\tau^*$
r	radial distance
r^+	radial distance in law-of-the-wall form = $r^* u_\tau^*/\nu^*$
r_o	body radius
Re	Reynolds number = $U_\infty^* L^*/\nu^*$
u	velocity component in x-direction
u^+	velocity in law-of-the-wall form = u^*/u_τ^*
u_τ^*	friction velocity (dimensional) = $(\tau_w^*/\rho^*)^{1/2}$
u_e	inviscid velocity at body surface
U_∞^*	free-stream velocity (dimensional)
x	arc length distance along body
x^+	arc length distance in law-of-the-wall form = $x_\tau^* u/\nu^*$
x_o	axial distance
y	distance normal to body surface
y^+	normal distance in law-of-the-wall form = $y^* u_\tau^*/\nu^*$
δ	boundary-layer thickness
Δ^*	mass deficit area = $\int_o^\infty (1 - \frac{u}{u_e}) r dy$
ε	eddy viscosity
ν^*	kinematic viscosity (dimensional)
κ	body longitudinal curvature

Nomenclature (continued)

ϕ angle between tangent to body surface and x_o - direction

ρ^* density (dimensional)

Θ momentum deficit area = $\int_o^\infty \frac{u}{u_e}(1 - \frac{u}{u_e})rdy$

τ^* shear stress in boundary layer (dimensional)

τ_w^* wall shear stress (dimensional)

All other quantities are defined in the text.

All quantities in the text, unless otherwise specified, are made dimensionless as follows:

distances with respect to L^*

velocity with respect to U_∞^*

pressure with respect to $\rho^* U_\infty^{*2}$

List of Figures

List of Figures (continued)

List of Table

Introduction

This report addresses the problem of improving the detailed predictions of thick axisymmetric turbulent boundary layers using a standard finite difference calculation scheme and a two-piece algebraic turbulence model. The typical result of such calculations is that in the vicinity of the tail the mean velocity profiles are too full close to the wall which is a reflection of the Reynolds stress being much too high across the boundary layer. The cause of this erroneous behavior is the use of a turbulence model which accounts for only the thin boundary-layer rate of strain proportional to $\partial u/\partial y$ and neglects the extra rates of strain due to longitudinal and transverse curvature. The experimental work of Patel and Lee [1]* has shown that these two extra rates of strain are extremely important in determining the turbulence properties in a thick axisymmetric boundary layer. They have also presented a method for the incorporation of these extra rates of strain in a one equation turbulence model and made calculations with their model which show excellent agreement with experiment. In this report the extra rate of strain approach of Patel and Lee is modified for application to a standard two-piece algebraic turbulence model.

Turbulence Model

The Reynolds stress is treated by a simple mean field closure which in a thin boundary layer reduces to

$$-\overline{u^{*\prime} v^{*\prime}} = \rho^* \varepsilon^* \frac{\partial u^*}{\partial y^*}, \tag{1}$$

---

*Numbers in brackets denote References cited at the end of the report.

where ε^* is the eddy viscosity. A zero-equation, or algebraic, model is used where the eddy viscosity is related directly to the mean velocity. Such a model requires the boundary layer to be divided into an inner (wall) region and an outer (wake) region with a different equation for ε in each region, as a consequence of the two different length scales. The junction point between these two regions is taken, in the usual way, to be the value of y where the inner and the outer values of ε are equal.

Inner Eddy Viscosity

The expression used for the eddy viscosity in the inner region is the Prandtl mixing length formula extended to account for transverse curvature effects which are important in a thick axisymmetric boundary layer. The thin boundary-layer eddy viscosity formula is, in dimensionless form [2],

$$\varepsilon_i = Re\ \ell^2 \left|\frac{\partial u}{\partial y}\right| , \tag{2}$$

where ℓ is the mixing length and the subscript "i" denotes the inner eddy viscosity. Generalizing the derivation of Cebeci [3], the form of the inner eddy viscosity for a thick axisymmetric boundary layer is deduced from the axisymmetric streamwise momentum equation near the wall. For small pressure gradient this equation can be approximated by

$$\frac{\partial}{\partial y^*}(r^*\tau^*) = 0 , \tag{3}$$

which has the first integral

$$r^*\tau^* = r_o^*\,\tau_w^* . \tag{4}$$

With the aid of Eq. (1), the shear stress in a boundary layer, which is the sum of molecular and turbulent contributions, can be expressed as

$$\tau^* = (\mu^* + \rho^*\varepsilon^*)\frac{\partial u^*}{\partial y^*} . \tag{5}$$

Equation (10) is a generalization of the form discovered by Rao which reduces to his expression when $\phi = 0$ (when the body is a cylinder or when it has a point of zero slope). In the form used by Cebeci for Y^+, $\cos\phi$ is omitted. Strictly speaking, Eq. (10) is valid only for small pressure gradient and hence ϕ cannot be very large (say, less than 0.2).

Since Y^+ formally transforms a thick axisymmetric boundary layer into a two-dimensional one, we can obtain the eddy viscosity for the thick axisymmetric case by substituting Y^+ for y^+ in the two-dimensional expression. Thus ε_i for a thick axisymmetric boundary layer is

$$\varepsilon_i = \ell^{+2} \frac{r^+}{r_o^+} \frac{du^+}{dy^+} \quad . \tag{11}$$

The mixing length ℓ^+ in the viscous dominated region near the wall as well as in the law-of-the-wall region, is given by

$$\ell^+ = 0.41 Y^+ D, \tag{12}$$

where D is the Van Driest damping function which supresses the linear dependence of ℓ^+ on Y^+ near the wall. The expression for D is

$$D = 1.0 - \exp(-Y^+/A^+) \quad , \tag{13}$$

where A^+ is an effective sublayer thickness, sometimes referred to as the Van Driest damping parameter. The parameter A^+ determines the thickness of the sublayer and is a function of the pressure gradient and transpiration rate.

Sublayer Damping Parameter

The expression used here for A^+ is the one deduced from experimental data by Crawford and Kays [5], as follows:

$$A^+ = \frac{26.0}{a\left[v_w^+ + b\left(\frac{P^+}{1+cv_w^+}\right)\right] + 1.0} \tag{14}$$

Then Eq. (4) becomes

$$r^*(\mu^* + \rho^*\varepsilon^*) \frac{\partial u^*}{\partial y^*} = r_o^* \tau_w^* \quad ,$$

which in universal law-of-the-wall variables is

$$\frac{r^*}{r_o^+} (1 + \varepsilon) \frac{\partial u^+}{\partial y^+} = 1 \quad . \tag{6}$$

The thin boundary-layer counterpart of Eq. (6) is

$$(1 + \varepsilon) \frac{\partial u^+}{\partial y^+} = 1 \quad . \tag{7}$$

Rao [4] was the first to show experimentally, on a cylinder with its longitudinal axis aligned with the flow, that the law of the wall still holds provided the normal spatial variable is redefined appropriately. Mathematically Rao's discovery means that Eq. (6) can be transformed into Eq. (5) by a change of independent variable. If Y^+ denotes the new axisymmetric variable, then we require

$$\frac{\partial}{\partial y^+} = \frac{\partial}{\partial y^+} \frac{dy^+}{dy^+} = \frac{\partial}{\partial y^+} \frac{r^+}{r_o^+} \quad ,$$

and hence,

$$\frac{dy^+}{dY^+} = \frac{r^+}{r_o^+} \quad . \tag{8}$$

From the geometry of a thick axisymmetric boundary layer, as shown in Fig. 1,

$$r = r_o + y \cos \phi \quad . \tag{9}$$

Equation (9) allows Eq. (8) to be integrated yielding the axisymmetric law-of-the-wall variable

$$Y^+ = \frac{r_o^+}{\cos \phi} \ln \frac{r^+}{r_o^+} \quad . \tag{10}$$

where

$$a = \begin{cases} 9.0 \text{ if } v_w^+ < 0 \\ 7.1 \text{ if } v_w^+ \geq 0 \end{cases} , \tag{15}$$

$$b = \begin{cases} 4.25 \text{ if } P^+ \leq 0 \\ 2.90 \text{ if } P^+ > 0 \end{cases} , \tag{16}$$

$$c = \begin{cases} 10.0 \text{ if } P^+ \leq 0 \\ 0 \quad \text{if } P^+ > 0 \end{cases} , \tag{17}$$

and

$$P^+ = \text{pressure gradient parameter} = \frac{\nu^*}{\rho^* u_\tau^*} \frac{dp^*}{dx^*} ,$$

$$v_w^+ = \text{blowing/suction parameter} = \frac{v_w^*}{u_\tau^*} .$$

Equation (14) has been derived for boundary layers in near equilibrium where P^+ and v_w^+ vary at most slowly along the surface.

When rapid changes occur in P^+ or v_w^+, the sublayer does not adjust instantaneously to the new conditions. Thus A^+ will lag its equilibrium value. Since A^+ is a function of P^+ and v_w^+, Crawford and Kays have introduced lag equations for these parameters to allow A^+ a finite time (or distance) to adjust to a new equilibrium state. The lag equations are of the form

$$\frac{d\Phi^+}{dx^+} = \frac{\Phi_e^+ - \Phi^+}{C} , \tag{18}$$

where Φ^+ denotes either P^+ or v_w^+ and the subscript e, the equilibrium value. Thus Φ^+ is the effective value of P^+ or v_w^+ to be used in Eq. (14). The quantity C is a lag constant with the recommended value of 4000, according to Crawford and Kays.

Unfortunately, for a body of revolution Eq. (18) gives erroneous behavior near the tail. What happens is that $d\Phi^+/dx^+$ changes sign causing Φ^+ to diverge from Φ_e^+ which is physically unreasonable. The cause of the sign reversal is the use of x^+ as an independent variable. By definition,

$$x^+ = Re\ u_\tau\ x \quad . \tag{19}$$

As the tail is approached u_τ begins to fall rapidly to zero, as it must, so that x^+ reaches a maximum and decreases. At the maximum of x^+, the derivation $d\Phi^+/dx^+$ changes sign. This erroneous behavior can be easily corrected by the following slight modification of the lag equation:

$$\frac{d\Phi^+}{dx} = \frac{\Phi_e^+ - \Phi^+}{\bar{C}(x)} \quad , \tag{20}$$

where $$\bar{C}(x) = \frac{C}{Re\ u_\tau(x)} \quad . \tag{21}$$

Equation (20) contains the same characteristic length scale as Eq. (18) but because x is used as the independent variable no sign reversal occurs.

The two lag equations, (18) and (20), have been tested on a modified spheroid at a Reynolds number, based on chord length, of 1.262×10^6 with $v_w = 0$, corresponding to the experiment of Patel, Nakayama and Damian [6]. Boundary-layer calculations were made using a Cebeci and Smith type of finite difference code developed at ARL. The measured pressure distribution was used in the calculation. For this body x^+ has a maximum which occurs at $x \cong 0.77$. The variations of P^+ and P_e^+ with x are shown in Figs. 2 and 3 for Eqs. (18) and (20) respectively. The choppy character of P_e^+ exhibited in these figures is caused by numerical inaccuracy in computing dp/dx. Figure 2 shows clearly the divergence of P^+ from P_e^+ which occurs downstream of x_{max}^+

when Eq. (18) is used. When Eq. (20) is used, as shown in Fig. 3, P^+ lags P_E^+ in a plausible manner. We would expect the wall friction coefficient to be a sensitive measure to differences in A^+ and, hence, in P^+. Figure 4 reveals that the calculated values of c_f using Eqs. (18) and (20) are indistinguishable until x becomes larger than about 0.86. Beyond x = 0.874 the boundary-layer calculation using Eq. (18) failed to converge. As can be seen in Fig. 2, at x = 0.874, P^+ becomes negative and decreases very rapidly

An alternate expression for A^+ has been derived by Cebeci [2] as an extension of Van Driest's one-dimensional unsteady analogy and is given by

$$A^+ = \frac{26}{N} \quad , \tag{22}$$

where

$$N^2 = \frac{-P^+}{v_w^+}\left[1 - \exp(11.8v_w^+)\right] + \exp(11.8v_w^+) \quad . \tag{23}$$

Cebeci does not use lag equations for P^+ or v_w^+.

For the case of $v_w^+ = 0$, considered herein, the variation of A^+ with P^+ according to the empirical expression of Crawford and Kays, Eq. (14), and the analytical expression of Cebeci, Eq. (22), is shown in Fig. 5. The two expressions differ markedly for $P^+ \neq 0$ with the differences being largest for $P^+ < 0$ (favorable pressure gradient). Because Eq. (14) is a fit of experimental data, it was chosen for use over Eq. (22).

Outer Eddy Viscosity

In the outer portion of the boundary layer (law of the wake region) we have the choice of using a constant mixing length, as used by Crawford and Kays, or a constant eddy viscosity, as used by Cebeci. The choice between the two in the present instance was dictated by computational reasons.

The matrix associated with the finite difference form of the boundary-layer equations at a particular x-wise station becomes ill conditioned near

the outer edge of the layer for the constant mixing length formulation.

When a linear solver without pivoting is used the resulting velocity profile exhibits fluctuations (numerical noise) which make the location of the outer edge very difficult to determine. With the constant eddy viscosity formulation these fluctuations are absent which was the reason it was chosen. Later on the discovery was made that by using a solver with pivoting (which nearly doubles the computation time per profile) the fluctuations in the velocity profile for the constant mixing length formulation were effectively eliminated.

In the outer region of the boundary layer the eddy viscosity is taken to be constant using the form first suggested by Clauser and later modified by Cebeci for low Reynolds number effects [2].

$$\varepsilon_o = \mathrm{Re}\ \alpha\ u_e\ \delta_k^* \quad , \tag{24}$$

where the subscript o denotes "outer" eddy viscosity, and, δ_k^* = kinematic displacement thickness

$$\delta_k^* = \int_o^\infty (1 - \frac{u}{u_e})\ dy \quad , \tag{25}$$

and α is a dimensionless constant given by

$$\alpha = \alpha_o \frac{1 + \Pi_o}{1 + \Pi} \tag{26}$$

where $$\alpha_o = 0.0168 \tag{27}$$

$$\Pi_o = 0.55 \tag{28}$$

$$\Pi = \Pi_o\ [1 - \exp(-0.243\sqrt{z_1} - 0.298 z_1)] \tag{29}$$

$$z_1 = \frac{\mathrm{Re}_{\theta k}}{425} - 1 \tag{30}$$

and $Re_{\theta k}$ is the Reynolds number based on the kinematic Reynolds number, viz.

$$Re_{\theta k} = \frac{\theta_k^* u_e^*}{\nu^*} = Re\ \theta_k\ u_e \tag{31}$$

where

$$\theta_k = \int_0^\infty \frac{u}{u_e}\left(1 - \frac{u}{u_e}\right) dy \tag{32}$$

Some formulations also include an intermittency factor to account for the intermittent character of turbulence at the outer edge of the boundary layer. In the present formulation this factor is omitted as it has been found to have negligible effect on the velocity profile and other boundary-layer parameters.

Curvature Effects

The so-called thick boundary-layer formulation, discussed in the section on the inner eddy viscosity, although necessary in defining the correct boundary-layer thickness, gives inadequate results for the details of the boundary layer as the tail of an asymmetric body is approached. The predicted Reynolds stress is always much too large and the resulting velocity profiles, therefore, much too full. Many investigators have noted this deficiency [1, 6, 7].

This defect in axisymmetric boundary-layer calculations, as mentioned in the introduction, may be traced to the neglect of the extra rates of strain due to transverse and longitudinal curvature which produce important extra terms in the Reynolds stress. A good bibliography of the experimental work on the effects of curvature on turbulence as well as a discussion of the dynamics of the problem may be found in the report by Patel and Lee [1].

Bradshaw [8] proposed a relation to account for the effect of extra rate of strain in a thin shear layer. His proposal was a linear modification of the turbulent length scale, valid for small extra rate of strain, as follows:

$$\frac{\ell}{\ell_o} = 1 + \frac{\hat{\alpha} e}{\frac{\partial u}{\partial y}} \quad , \tag{33}$$

where ℓ_o is the length scale (mixing length) associated with the rate of strain $\partial u/\partial y$, ℓ is the length scale with extra rate of strain e included and $\hat{\alpha}$ is a constant of order 10. Bradshaw also proposed that the equilibrium value of e in Eq. (33) be replaced by an effective e to account for rapid changes in the boundary-layer history. The effective e, denoted by e_{eff}, is then governed by a lag equation,

$$\frac{d}{dx}(e_{eff}) = \frac{1}{L_e}(e - e_{eff}) \quad , \tag{34}$$

where Le is a lag length for the boundary layer response to changes in e. The suggested value of L_e is 10δ.

Bradshaw recognized that, in general, e would be a function of y as well as x. To get around this difficulty, since Eq. (34) is an ordinary differential equation in x, he suggests removing the y-dependency in e by using e/u in Equation (34) in cases where $e \propto u$ such as curvature, lateral divergence and bulk compression.

Patel and Lee [1] have incorporated Bradshaw's ideas concerning curvature effects into an axisymmetric finite difference boundary layer calculation scheme with a one-equation transport model for the turbulent shear stress. Comparisons of their own extensive data for the two body shapes with different curvature histories with the calculations show

very good agreement when both longitudinal and transverse extra rates of strain are included. The extra rates of strain in these calculations are not small so that Bradshaw's linear formula breaks down, leading to a very rapid decrease in ℓ across the boundary layer and thus to a near total destruction of the Reynolds stress. To correct this situation they propose the following nonlinear formula:

$$\frac{\ell}{\ell_o} = \left[1 - \frac{\hat{\alpha}\, e_{eff}}{\frac{\partial u}{\partial y}}\right]^{-1} , \tag{35}$$

which reduces to Bradshaw's linear formula when $\hat{\alpha}\, e_{eff}/u_y$ is small.

Huang et al. [7] have suggested that the extra rates of strain in a thick axisymmetric boundary layer can be accounted for by the following simple formula:

$$\frac{\ell}{\ell_o} = \frac{[(1 + \delta/r_o)^2 - 1]^{1/2}}{3.33\ \delta/r_o} . \tag{36}$$

This formula is based on the idea that the square of the turbulent length scale is related to the annular area of the boundary layer. Huang's formula gives a uniform reduction of the two-dimensional mixing length across the entire boundary layer therefore producing too large a reduction in Reynolds stress in the wall layer region.

Incorporation of Curvature Effects in the Turbulence Model

The formula of Huang as well as a number of variations of the nonlinear formula of Patel and Lee were incorporated in the present two-piece algebraic turbulence model and applied to several axisymmetric bodies with different

curvature histories. The best formulation, as judged by agreement between the predicted results and experiment, was found to be the following modification of the formula of Patel and Lee:

$$\frac{\ell}{\ell_o} = (1 - f\hat{\Phi})^{-1} \tag{37}$$

where:
$$f = \hat{\alpha}\left[1 - \exp\left(\frac{-x+x_o}{5\delta_o}\right)\right] \tag{38}$$

$$\hat{\Phi} = \frac{1}{\frac{\partial u}{\partial y}}\,(e_t + e_\ell) \tag{39}$$

and e_t = transverse extra rate of strain

$$e_t = \frac{u}{1+ky}\,\frac{1}{r}\,\frac{\partial r}{\partial x} \tag{40}$$

e_ℓ = longitudinal extra rate of strain,

$$e_\ell = \frac{ku}{1+ky} \quad . \tag{40}$$

From Eq. (9) and the definition of body longitudinal curvature κ, we find that

$$\frac{\partial r}{\partial x} = \frac{dr_o}{dx} - \kappa y \sin\phi \ ,$$

and hence Eq. (39) can be written in the final form:

$$\hat{\Phi} = \frac{u}{\frac{\partial u}{\partial y}} \cdot \frac{1}{1+\kappa y}\left[\left(\frac{1-\kappa y}{r}\right)\sin\phi - r\right] \quad . \tag{42}$$

The manner of implementation is as follows:

1. The extra rate-of-strain effects are gradually switched on beginning at $x = x_o$, the station where $\delta > 0.1$, corresponding to where the thin boundary-layer formulation begins to break down.
2. The <u>exact</u> formulas for e_t and e_ℓ are used and a simple sum formed to account for both effects, as suggested by Patel and Lee.

3. No lag equation is used in conjunction with e_t or e_ℓ because none could be found that was universal for the range of geometries tested, and further, to separate out the x-dependency requires a separate lag equation for e_t/u and e_ℓ/u with the remaining y dependency omitted.

4. At a particular x-station, the thick boundary layer eddy viscosity (without extra rates of strain) is computed according to Eqs. (11), (12) and (24) and y_c found. Then the mixing length ratio ℓ/ℓ_o is computed from Eq. (37) for $0 \leq y \leq y_c$. From Eq. (11), $(\varepsilon_o)_i \sim \ell_o^2$ and hence the inner eddy viscosity, modified for extra rates of strain, is given by

$$\varepsilon_i = \lambda^2 (\varepsilon_o)_i \quad , \quad 0 \leq y \leq y_c \, , \tag{43}$$

where $\lambda = \frac{\ell}{\ell_o}$ is given by Eq. (37) and $(\varepsilon_o)_i$ is given by Eqs. (11) and (12). For $y_c \leq y \leq \delta$ the value of λ at $y = y_c$ is used, denoted by λ_c. Thus the modified outer eddy viscosity is

$$\varepsilon_o = \lambda_c^2 \, (\varepsilon_o)_o \quad , \quad y_c \leq y \leq \delta \quad , \tag{44}$$

and $(\varepsilon_o)_o$ is given by Eq. (24).

Results

The boundary layers on three bodies of revolution each having a different longitudinal curvature history, have been calculated with the ARL finite difference boundary-layer code using the foregoing algebraic turbulence model with and without extra rates of strain. For each of these bodies a sufficient amount of detailed experimental measurements exists with which to make comparisons. The bodies are:

1. F-57 low drag body, ref. 1
2. Modified spheroid, ref. 6
3. NSRDC body (afterbody no. 1), ref. 7

Case	Chord Reynolds Number	Boundary-Layer Trip-Location*	Transition Location in Calculations*	No. Normal Steps at Stag. Pt.	No. Streamwise Stations
F-57	1.20×10^6	0.474	0.300	30	112
Spheroid	1.26×10^6	0.048	0.050	30	111
NSRDC	6.60×10^6	0.050	0.015	30	107

*Fraction of chord length measured from nose along centerline.

TABLE 1. BOUNDARY-LAYER INPUT PARAMETERS

30 September 1982
GHH:cfb

The geometries are shown in Figs. 6-8.

Boundary-layer input parameters for the three cases are listed in Table 1. Transition locations in the calculations were chosen so that Θ in the laminar-turbulent region closely fitted the experimental data. For the step size in the direction normal to the body surface a geometric progression was used where the transformed step size ratio was taken to be 1.10. At the stagnation point boundary-layer infinity was taken to be $\eta_\infty = 5.0$, where η is the Mangler-Levy-Lees variable defined by Eq. (7.3.4) of ref. 2. The pressure distribution in each case, obtained by the Douglas Neumann procedure, was modified in the stern region to coincide with the experimental measurements. All cases were run on a VAX 11/780 computer using double precision arithmetic.

The tuning of the modified turbulence model was performed using the F-57 and modified spheroid data only. The best agreement with these data was found when the constant $\hat{\alpha}$ in Eq. (38) had the value 3.0. The solution for the NSRDC body was then run using this value of $\hat{\alpha}$. In all three cases solutions were also obtained using the unmodified turbulence model ($\hat{\alpha} = 0$).

The reason for using the F-57 and modified spheroid in the turbulence model tuning process, aside from the high quality of the data, is that these bodies have very different longitudinal curvature histories. Consequently, the contributions of e_t and e_ℓ to the individual boundary layers will be different.

For the F-57 and modified spheroid, mean velocity profiles, Reynolds stress profiles, skin friction coefficient, boundary layer shape factor and momentum deficit area are presented, whereas, for the NSRDC body only mean

velocity profiles and skin friction coefficient are given. Comparisons of calculations with experiment for the F-57 body appear in Figs. 9-17, for the modified spheroid in Figs. 18-28 and for the NSRDC body in Figs. 29-32.

For the F-57 body calculations near the stern using the modified turbulence model are in better agreement with experiment for the mean velocity and Reynolds stress profiles than corresponding calculations with the unmodified model (see Figs. 9-14). At the last station, $x_o = 0.96$, the modified turbulence model suppresses the Reynolds stress too much near the wall and produces an overcorrection in the velocity profile. Nevertheless, the modified result is still in better agreement with experiment than the unmodified one. Suprisingly enough, the shape of the Reynolds stress profile is qualitatively correct for the modified model.

The modified model reduces the skin friction coefficient slightly below the measured values, as shown in Fig. 15, indicating that ℓ/ℓ_o, as given by Eq. (37), is decreasing too rapidly near the wall. One possible way of suppressing this rapid drop off would be to use a damping factor in Eq. (37), similar to Eq. (13). As seen in Figs. (16) and (17), the shape factor prediction is improved somewhat by the modification while the momentum deficit area remains almost unchanged, as would be expected.

In the case of the modified spheroid, for mean velocity and Reynolds stress, as shown in Figs. 19-25, the modified turbulence model gives results in better agreement with experiment than those of the unmodified model. Here the improvement is not quite as dramatic as in the case of the F-57 body, except at the last station, $x_o = 0.99$. The agreement can be improved by increasing $\hat{\alpha}$ to about 3.5 or 4.0, but then the results for the F-57 body become worse because the correction becomes too large near the tail.

In Figs. 26 and 27 the modification is seen to improve agreement for the skin friction coefficient and shape factor. The momentum deficit area, shown in Fig. 28, is essentially unchanged by the modification, as was the case for the F-57.

The mean velocity profile measurements given in ref. 7 for the NSRDC body are in cylindrical coordinates (x_o, r) with corresponding velocity components (u_x, v_r). To obtain calculated velocity profiles in cylindrical coordinates required the use of double quadratic interpolation plus the usual axis rotation. The mean velocity profile comparisons are shown in Figs. 29-31. As in the previous two cases, the modified turbulence model gives results which are in very good agreement with the experimental data and are superior to the results of the unmodified model. Finally, in Fig. 32 the modification is seen to lower the skin friction coefficient as much as 20 percent below the measured values. This situation is the same as occurred for the F-57 body (see Fig. 15).

Conclusions

1. The inclusion of extra rates of strain in a two piece algebraic turbulence model has been found to provide a definite improvement in the prediction of mean velocity and Reynolds stress profiles as well as shape factor in the tail region of an axisymmetric boundary layer.
2. Both longitudinal and transverse extra rates of strain must be incorporated in the turbulence model to produce best agreement with experiment. In the present treatment the equilibrium values of e_t and e_ℓ are added together to form an effective e which is then used in a simple nonlinear length scale ratio formula to modify the mixing length. This formulation, a modification of a scheme proposed by Patel and Lee, has been found to be the best of several tried.

3. The best value of the empirical constant $\hat{\alpha}$ in Eq. (37) for the length scale ratio has been found by numerical experiments to be 3.0.

4. The predicted skin friction coefficient distribution in the vicinity of the tail, as given by the turbulence model modified for extra rates of strain, has been found to lie generally below measured values. This defect appears to be related to the overly rapid decay of length scale ratio near the wall. A possible remedy is to employ a damping function, similar to Eq. (13), in the vicinity of a wall.

The axisymmetric boundary-layer computer code with the modified turbulence model described in this report is available from the author.

References

[1] Patel, V. C. and Lee, Y. T., "Thick Axisymmetric Turbulent Boundary Layer and Near Wake of a Low-Drag Body of Revolution", Report No. 210, Iowa Institute of Hydraulic Research, Iowa City, Iowa, Dec. 1977.

[2] Cebeci, T. and Bradshaw, P., Momentum Transfer in Boundary Layers, McGraw-Hill, New York, 1977, Chap. 6.

[3] Cebeci, T. and Smith, A. M. O., Analysis of Turbulent Boundary Layers, Academic Press, New York, 1974, Chap. 6.

[4] Rao, G. N. V., "The Law of the Wall in Thick Axisymmetric Turbulent Boundary Layers", Jour. Applied Mech., 89, 327 (1967).

[5] Crawford, M. E. and Kays, W. M., "STAN5-A Program of Numerical Computation of Two-Dimensional Internal and External Boundary Layer Flows", NASA CR-2742, National Aeronautics and Space Administration, Washington, D. C., Dec. 1976.

[6] Patel, V. C., Nakayama, A. and Damian, R., "Measurements in the Thick Axisymmetric Boundary Layer Near the Tail of a Body of Revolution", Jour. Fluid Mech., 63, 345 (1974).

[7] Huang, T. T., Santelli, N. and Belt, G., "Stern Boundary-Layer Flow on Axisymmetric Bodies", presented at Twelfth Symposium on Naval Hydrodynamics, Washington, D. C., 5-9 June 1978.

[8] Bradshaw, P., "Effects of Streamline Curvature on Turbulent Flow", AGARDograph No. 169 (1973).

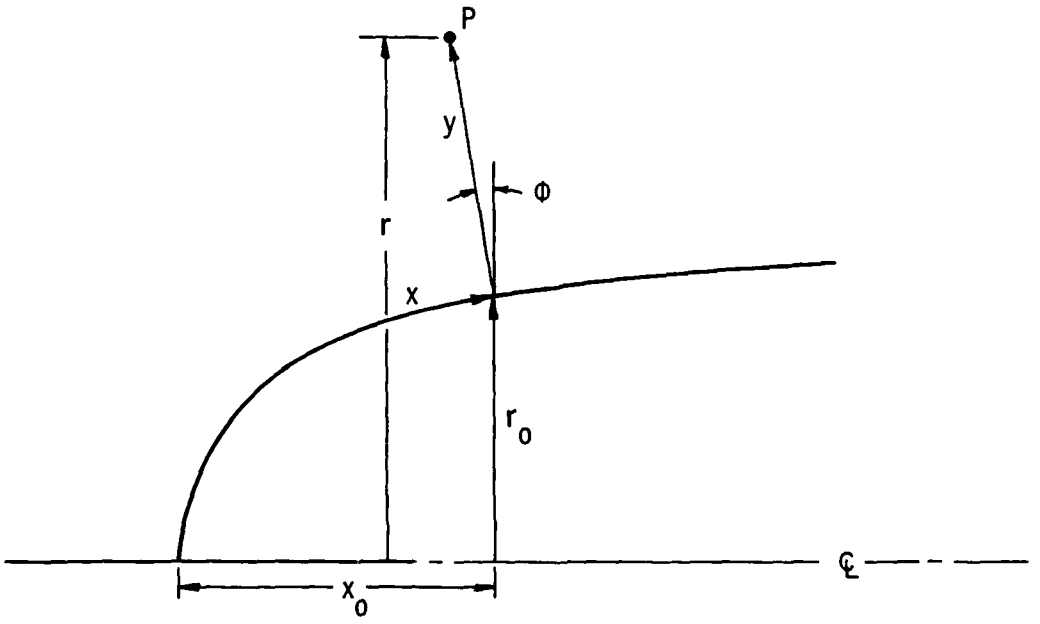

Figure 1. Coordinate System for a Thick Axisymmetric Boundary Layer.

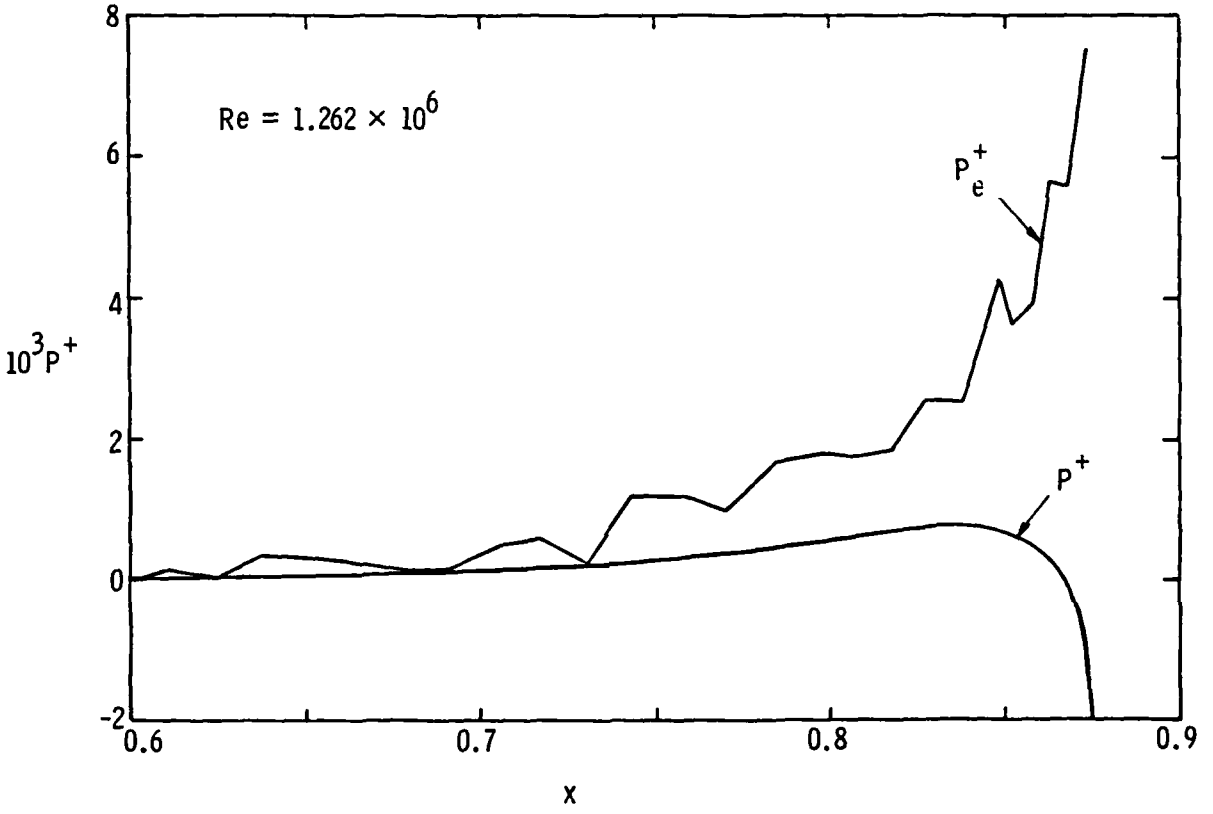

Figure 2. Unmodified Lag Equation for P^+, Modified Spheroid.

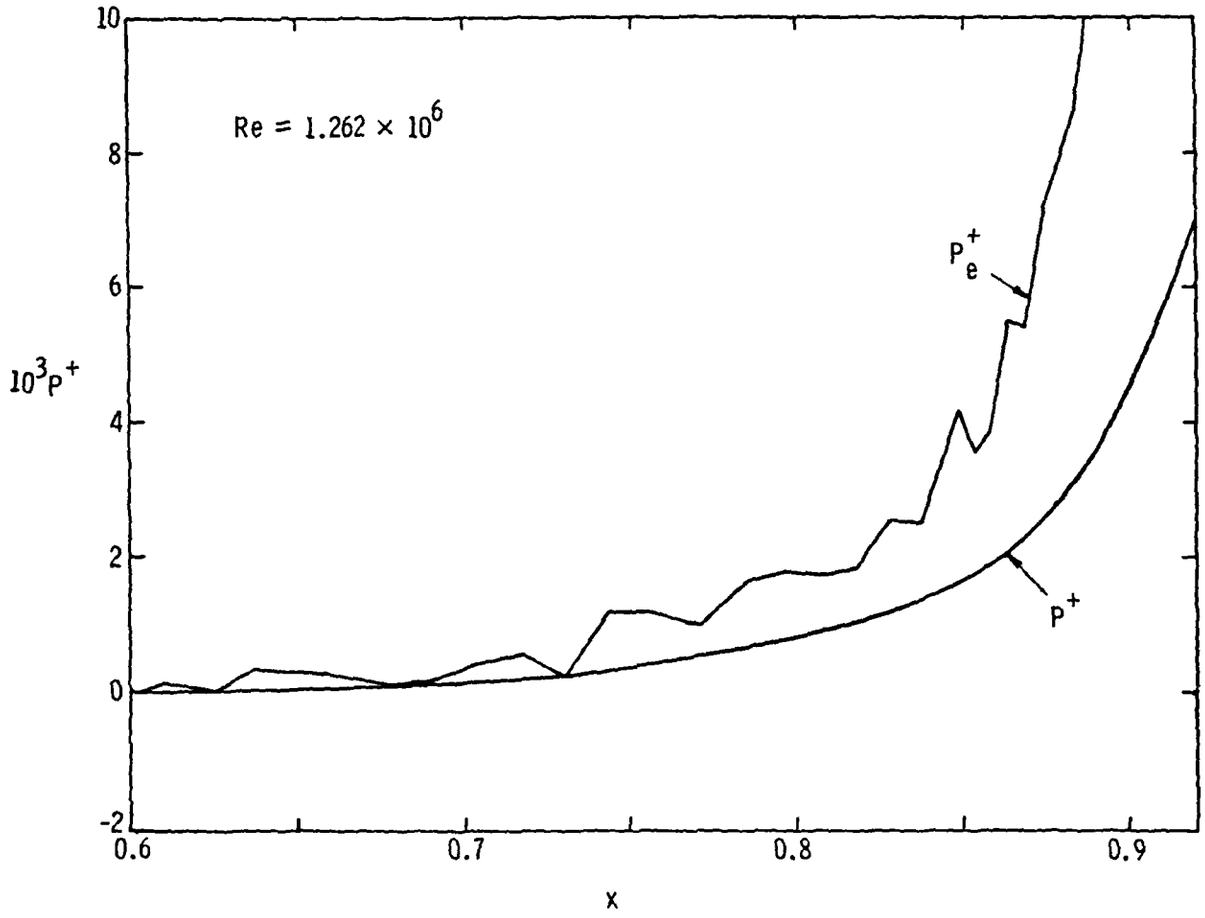

Figure 3. Modified Lag Equation for P^+, Modified Spheroid.

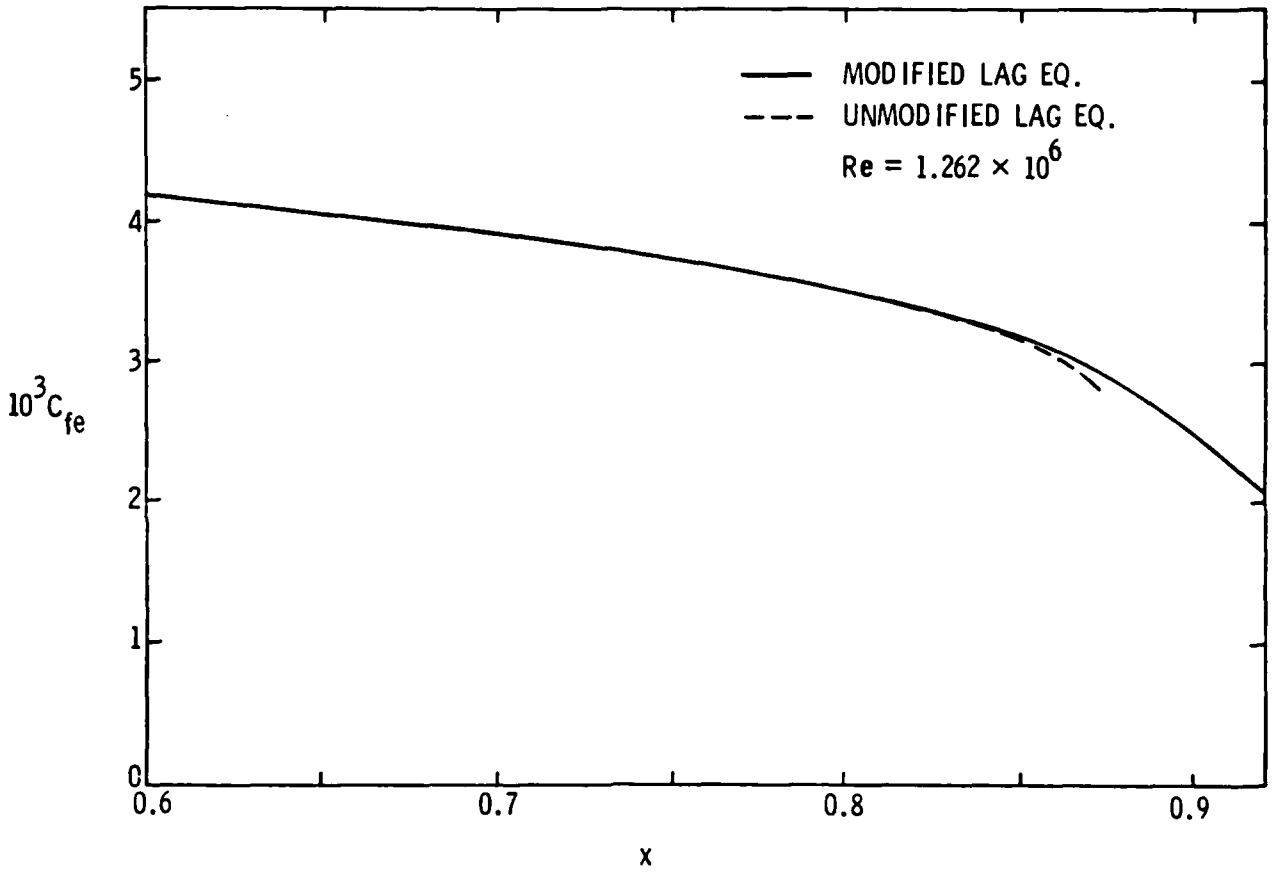

Figure 4. Skin Friction Coefficient on Modified Spheroid.

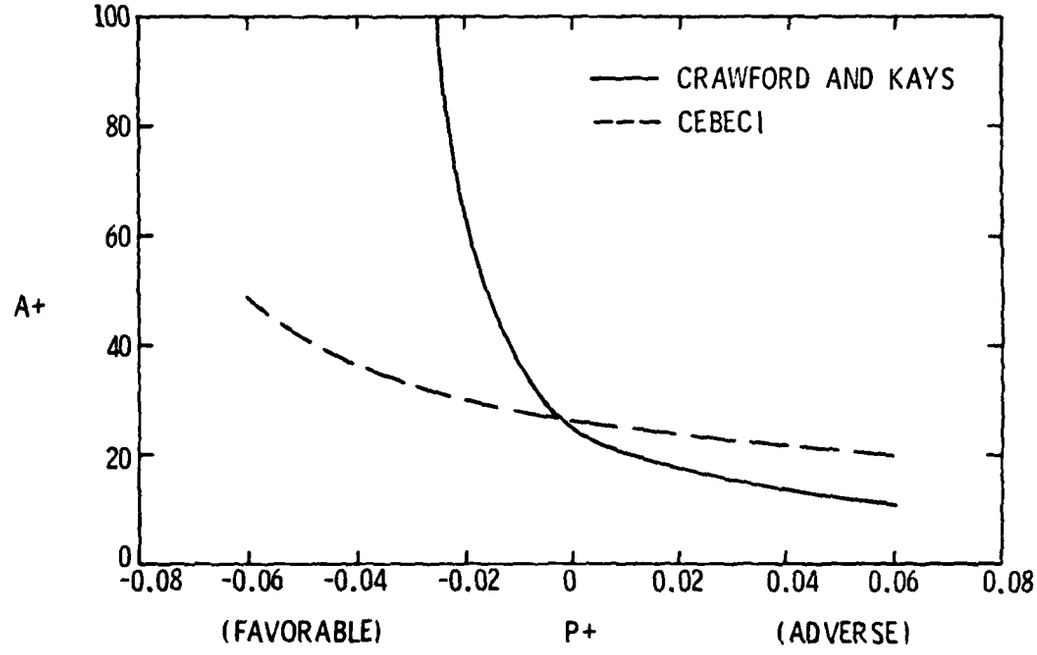

Figure 5. Variation of Sublayer Thickness Parameter with Pressure Gradient, Impervious Wall.

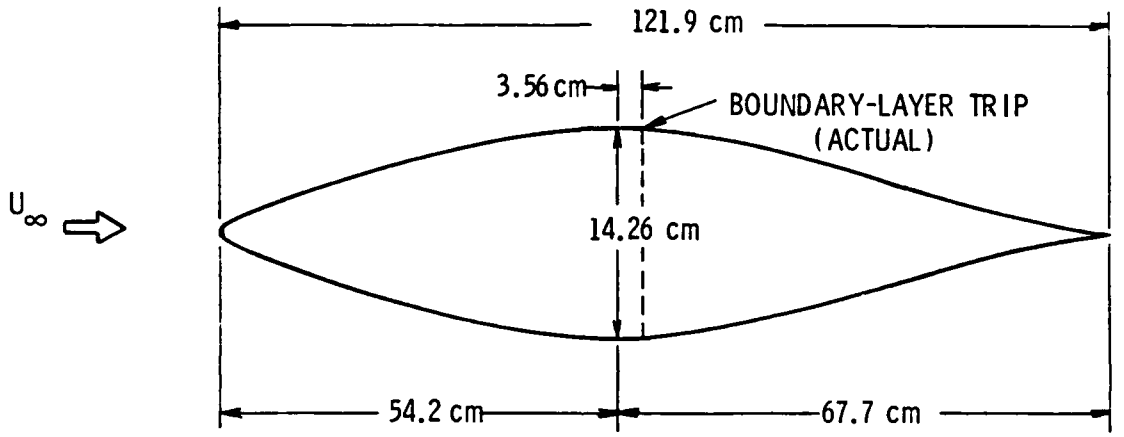

Figure 6. F-57 Geometry.

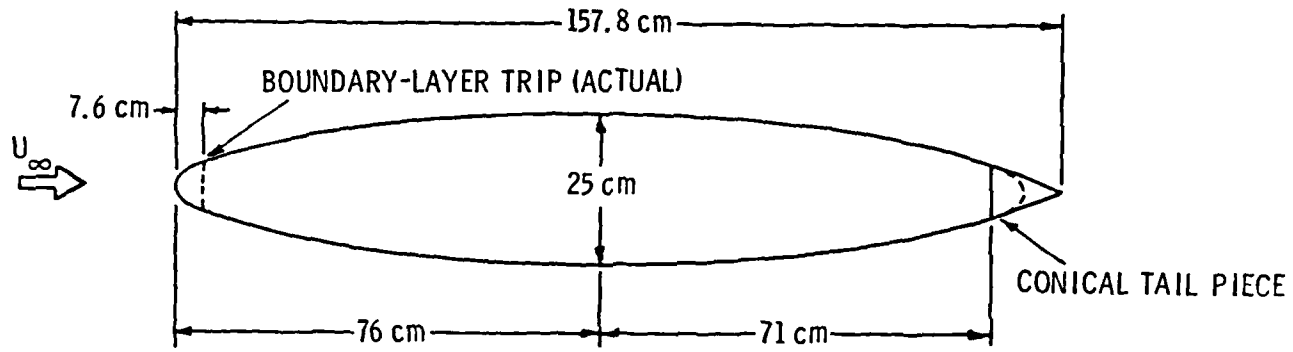

Figure 7. Modified Spheroid Geometry.

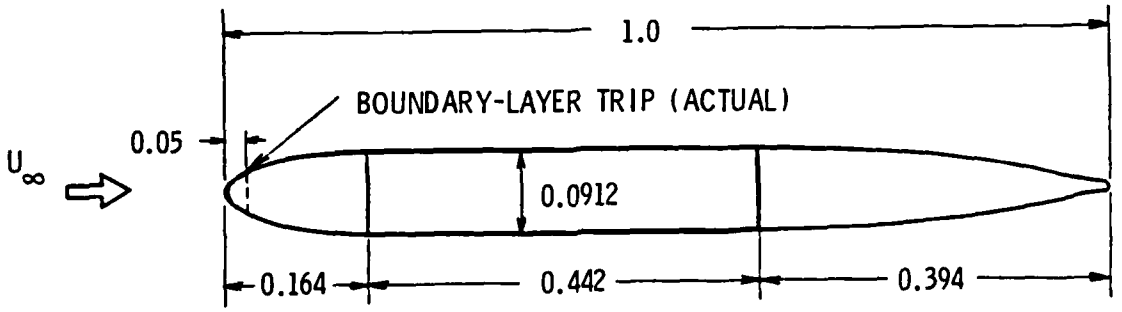

Figure 8. NSRDC Body Geometry.

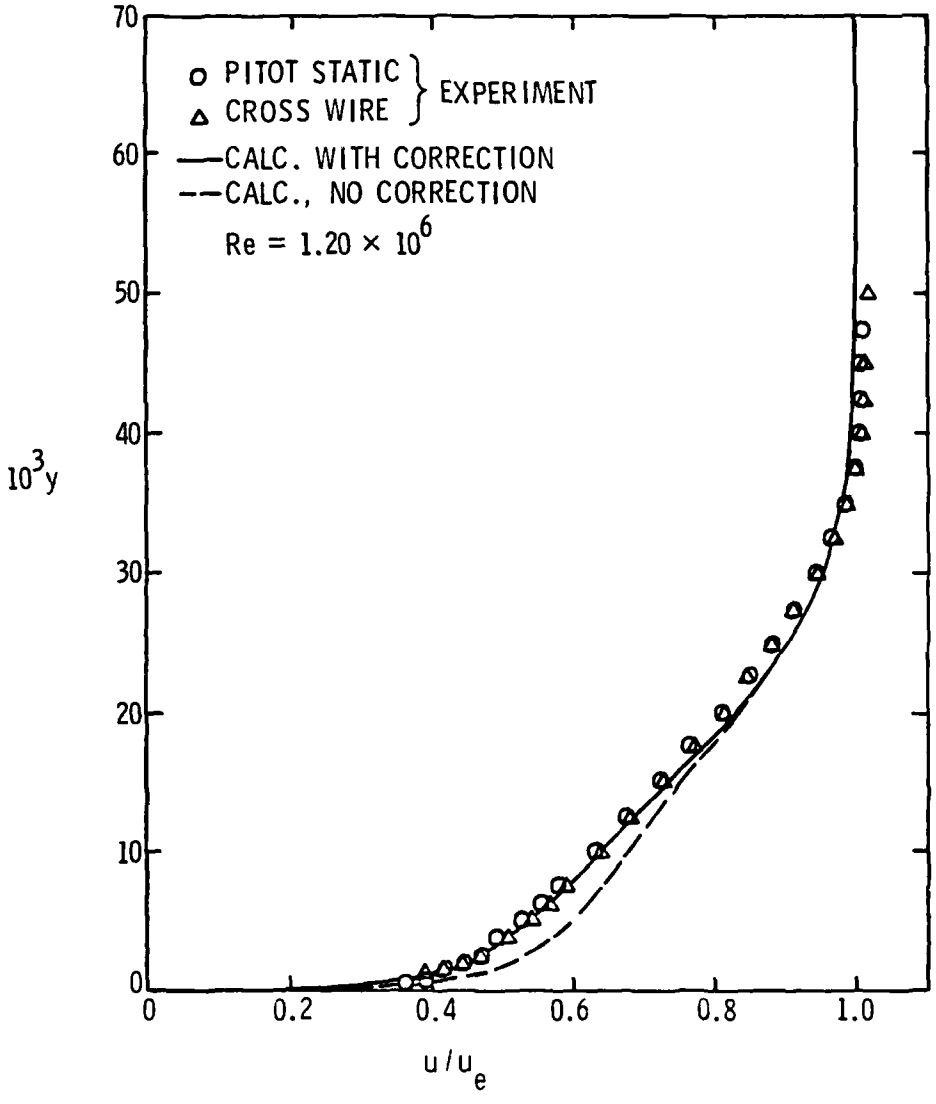

Figure 9. Mean Velocity Profile at x_o = 0.88, F-57 Body.

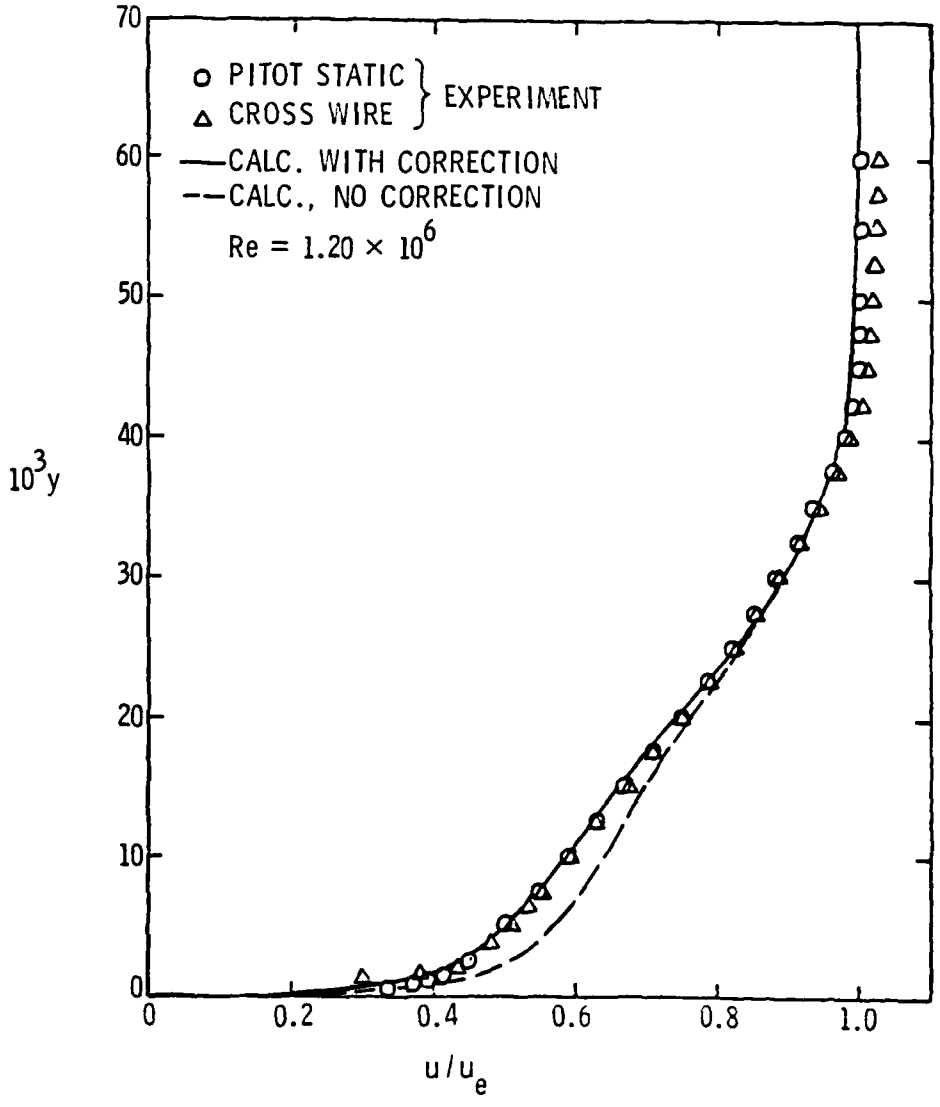

Figure 10. Mean Velocity Profile at x_o = 0.92, F-57 Body

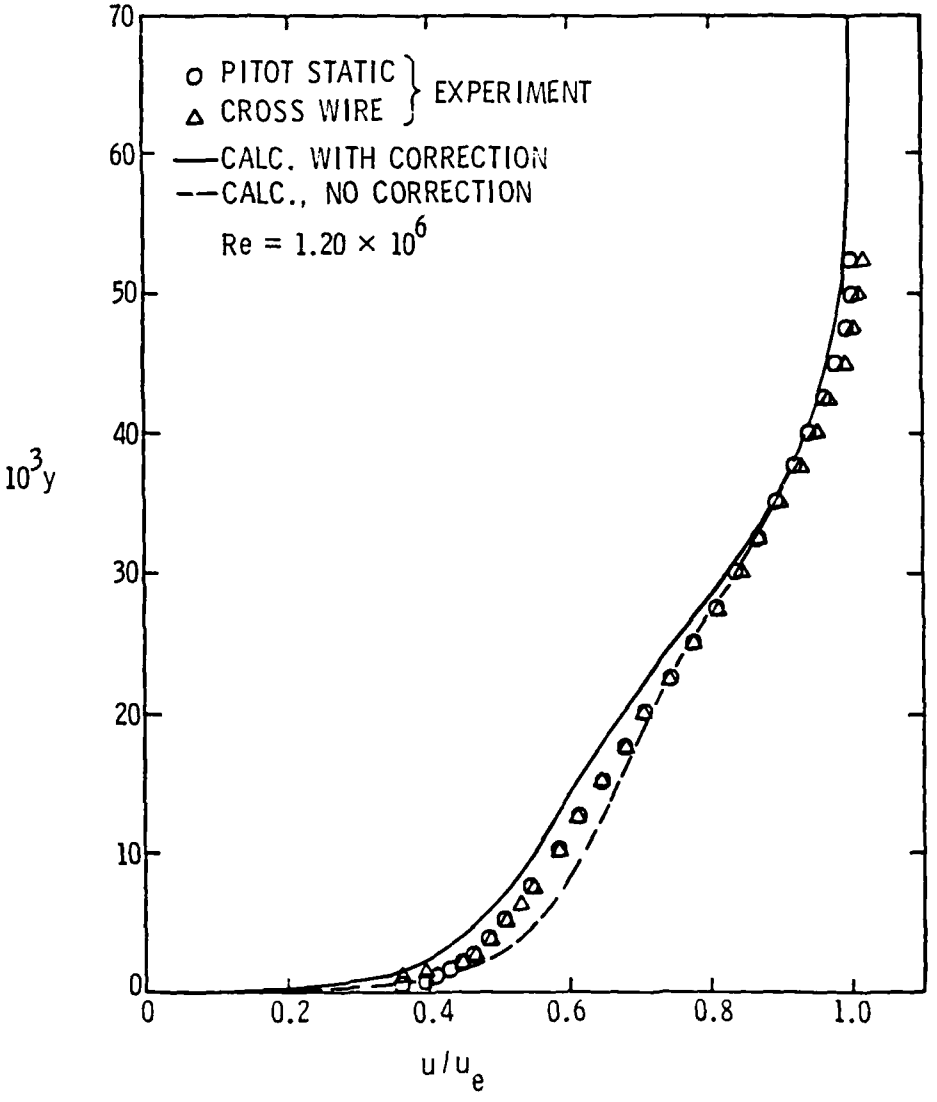

Figure 11. Mean Velocity Profile at x_o = 0.96, F-57 Body.

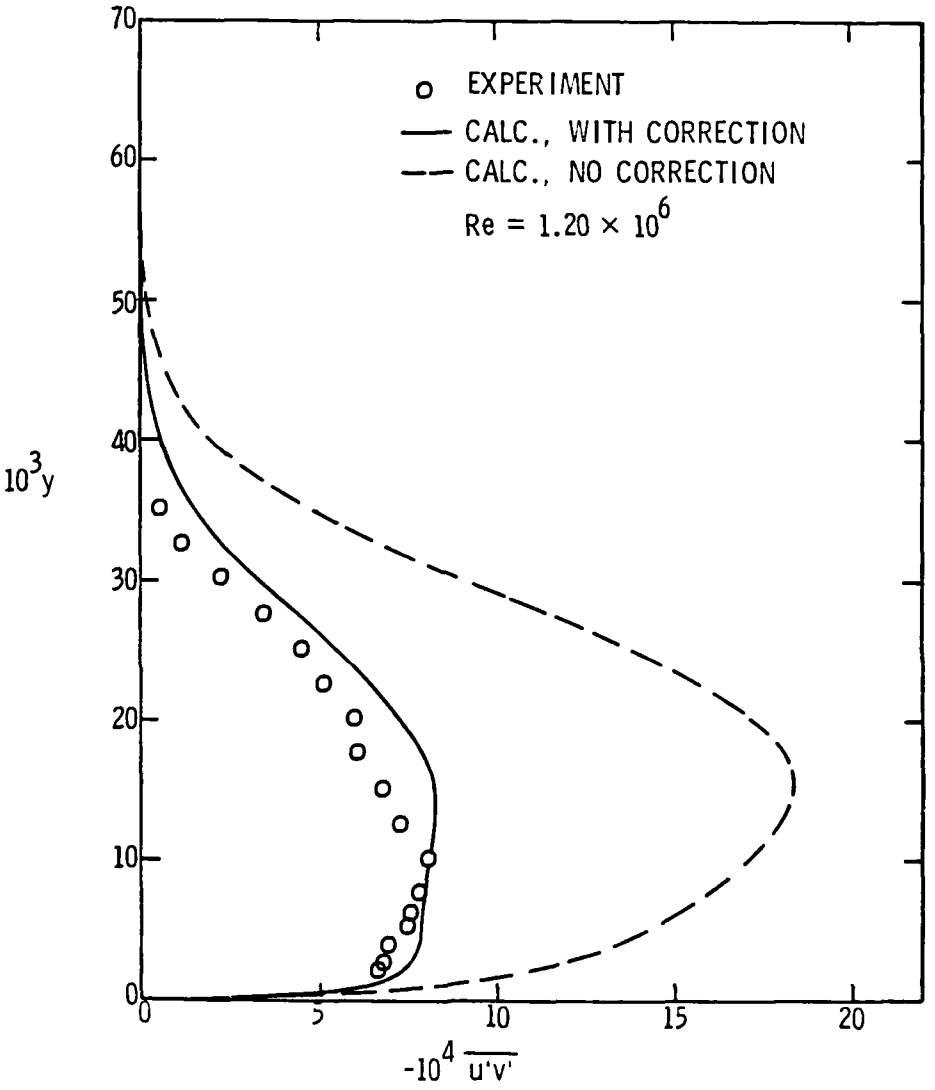

Figure 12. Reynolds Stress Profile at x_o = 0.88, F-57 Body.

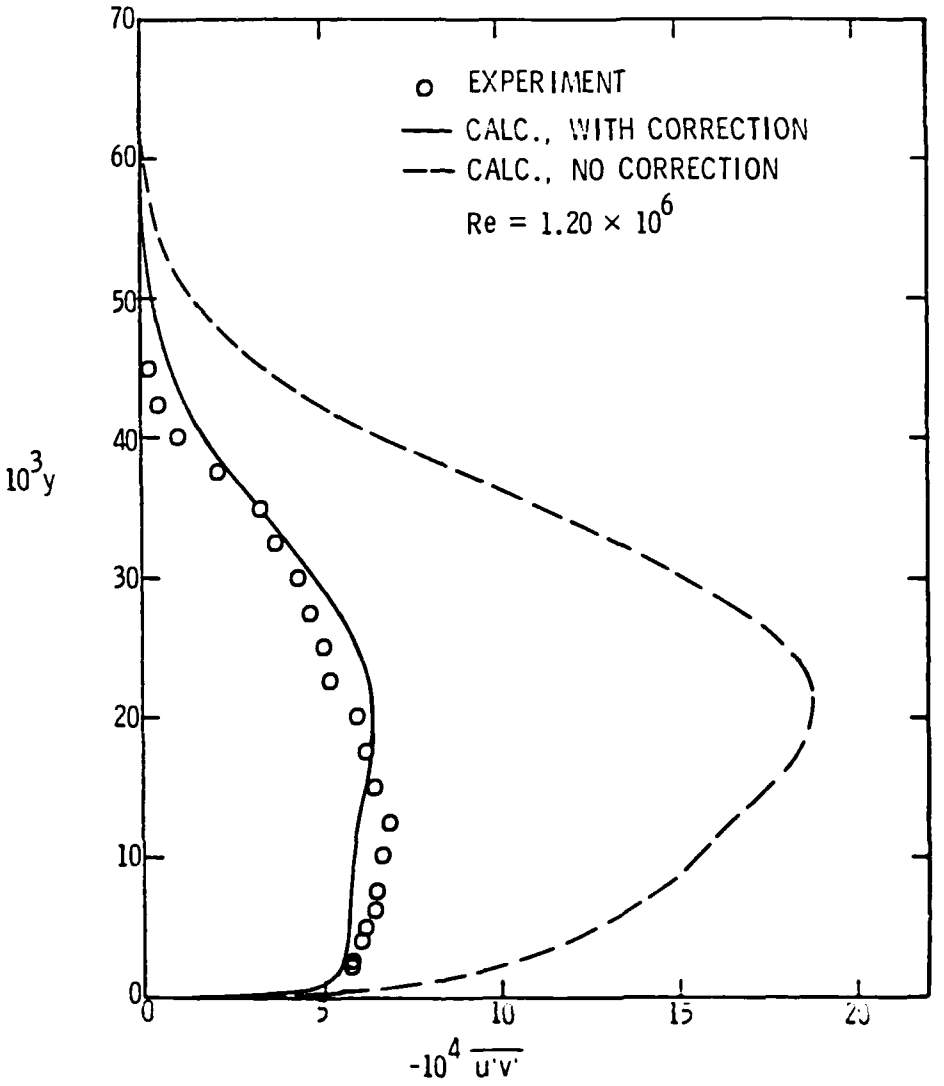

Figure 13. Reynolds Stress Profile at x_o = 0.92, F-57 Body.

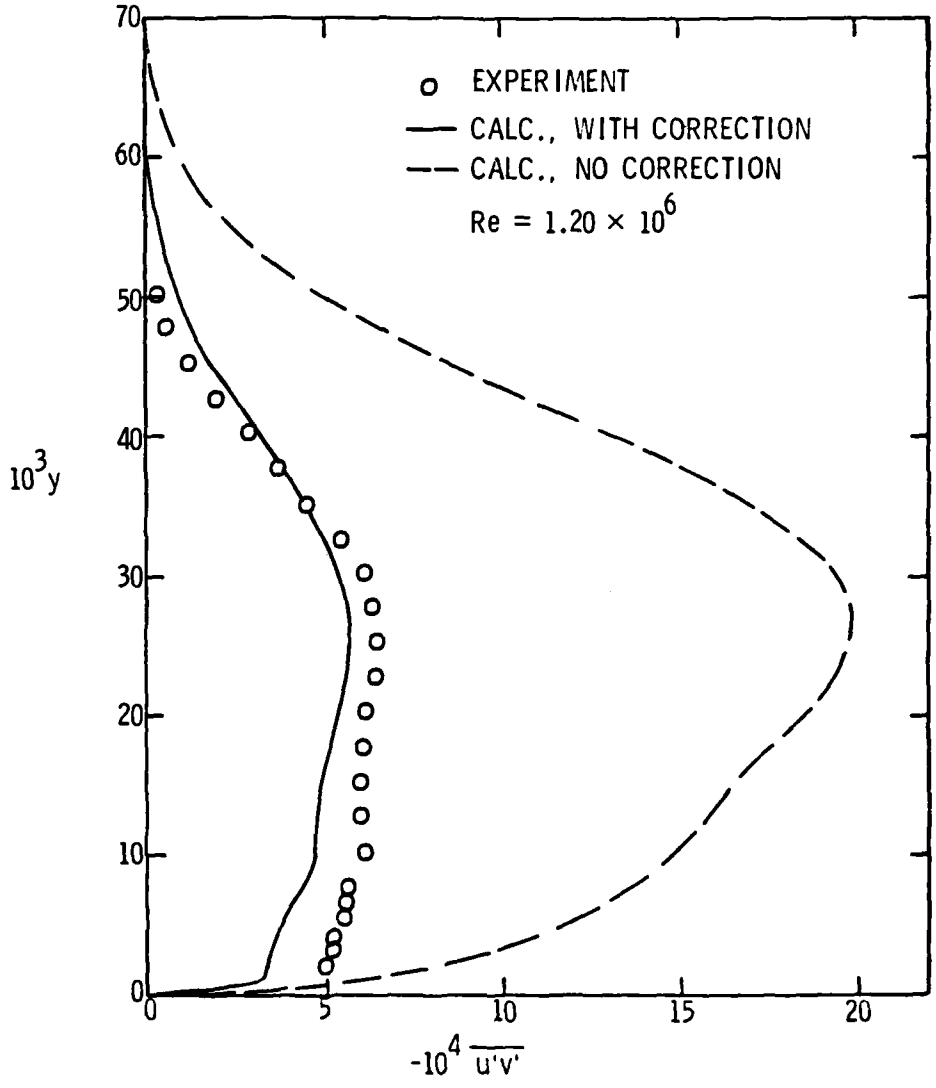

Figure 14. Reynolds Stress Profile at x_o = 0.96, F-57 Body.

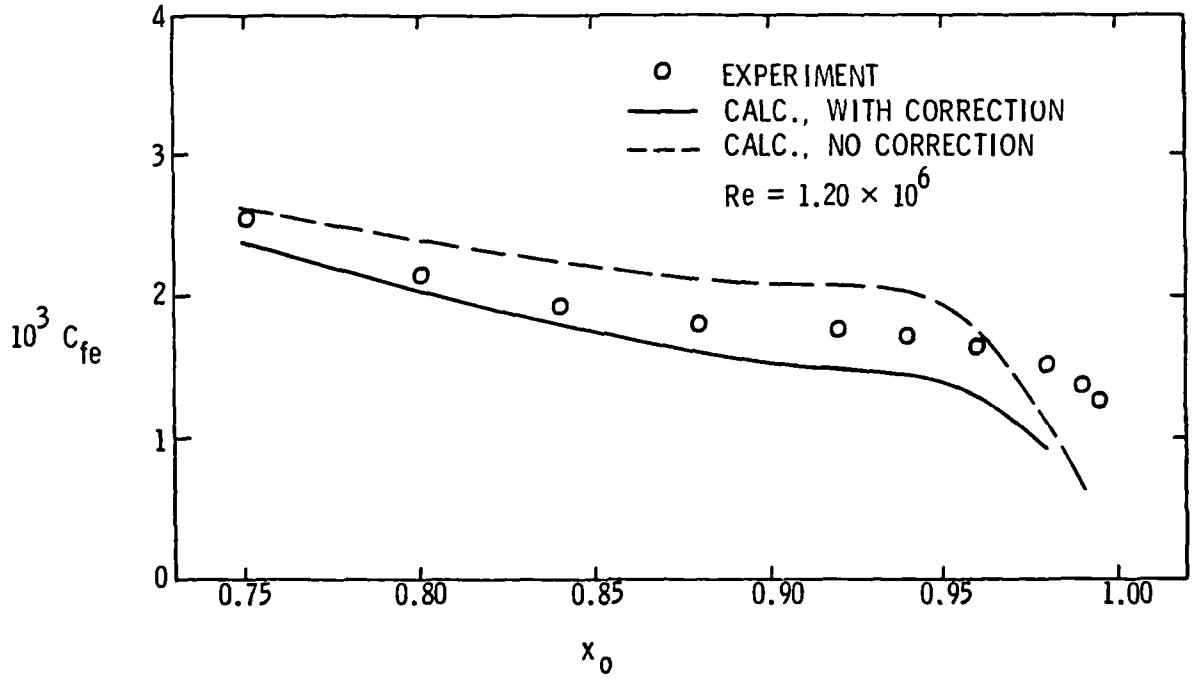

Figure 15. Skin Friction Coefficient Distribuiton, F-57 Body.

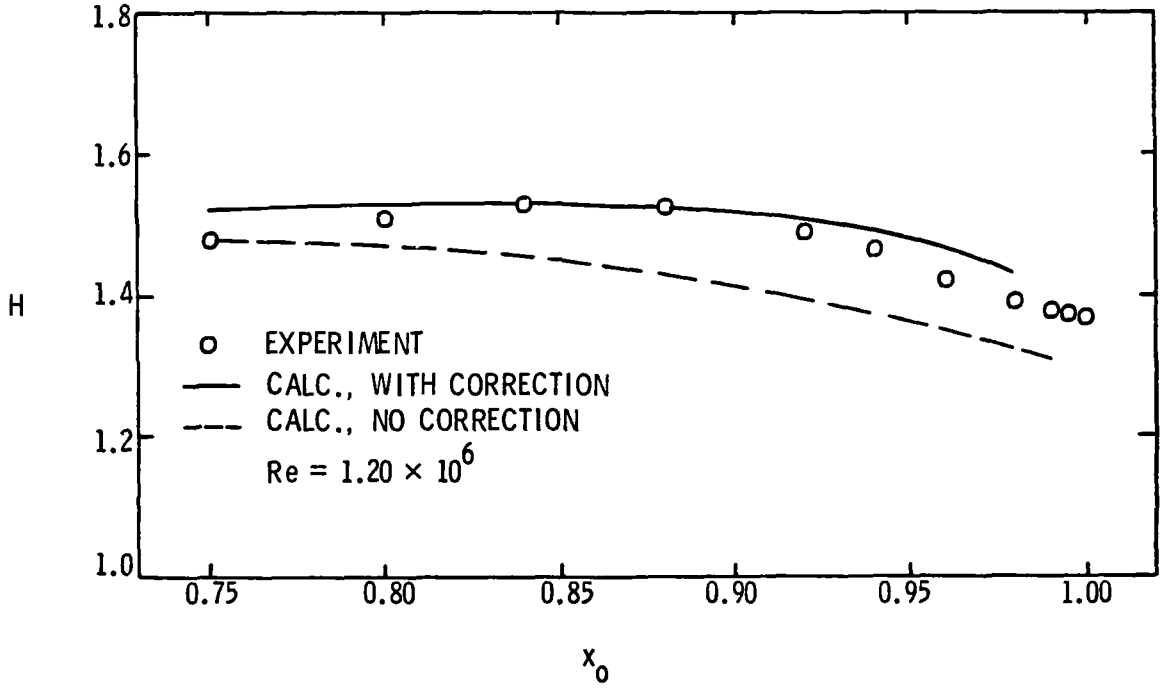

Figure 16. Shape Factor Distribution, F-57 Body.

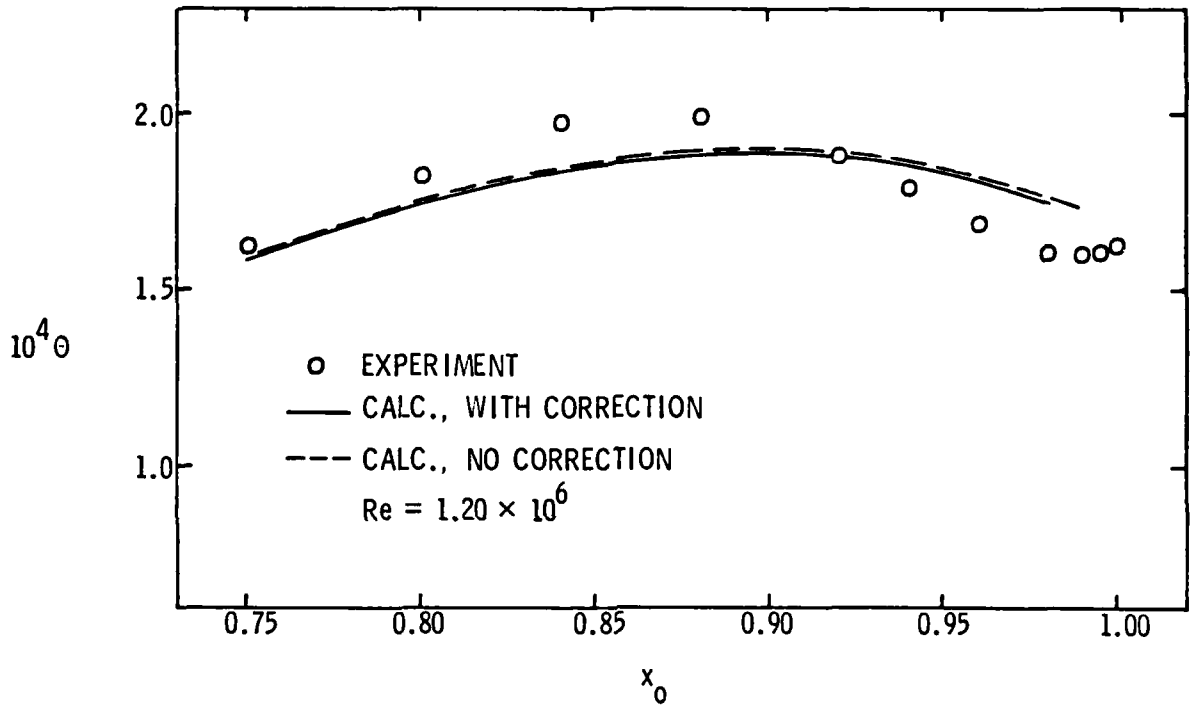

Figure 17. Momentum Deficit Area Distribution, F-57 Body.

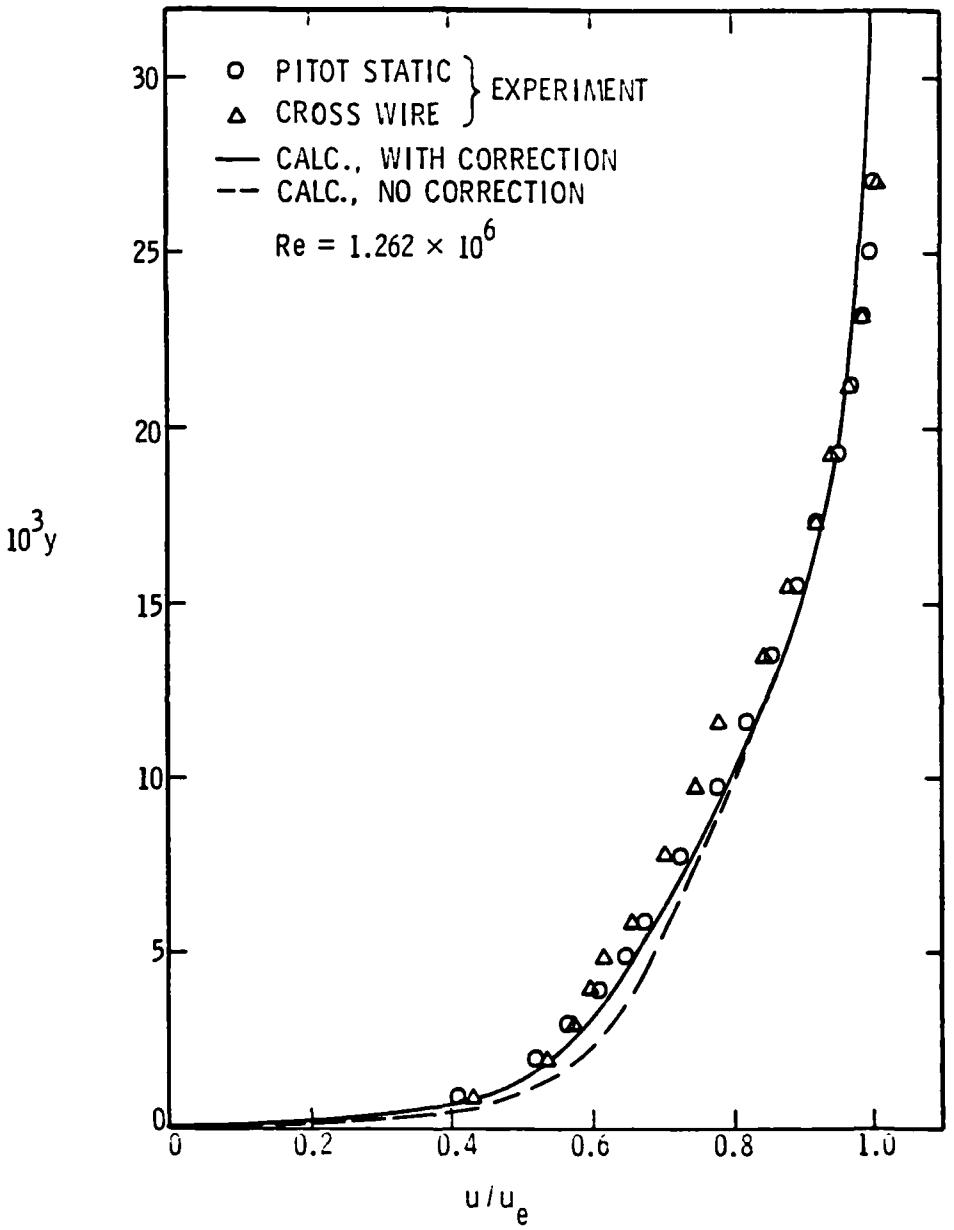

Figure 18. Mean Velocity Profile at x_o = 90, Modified Spheroid.

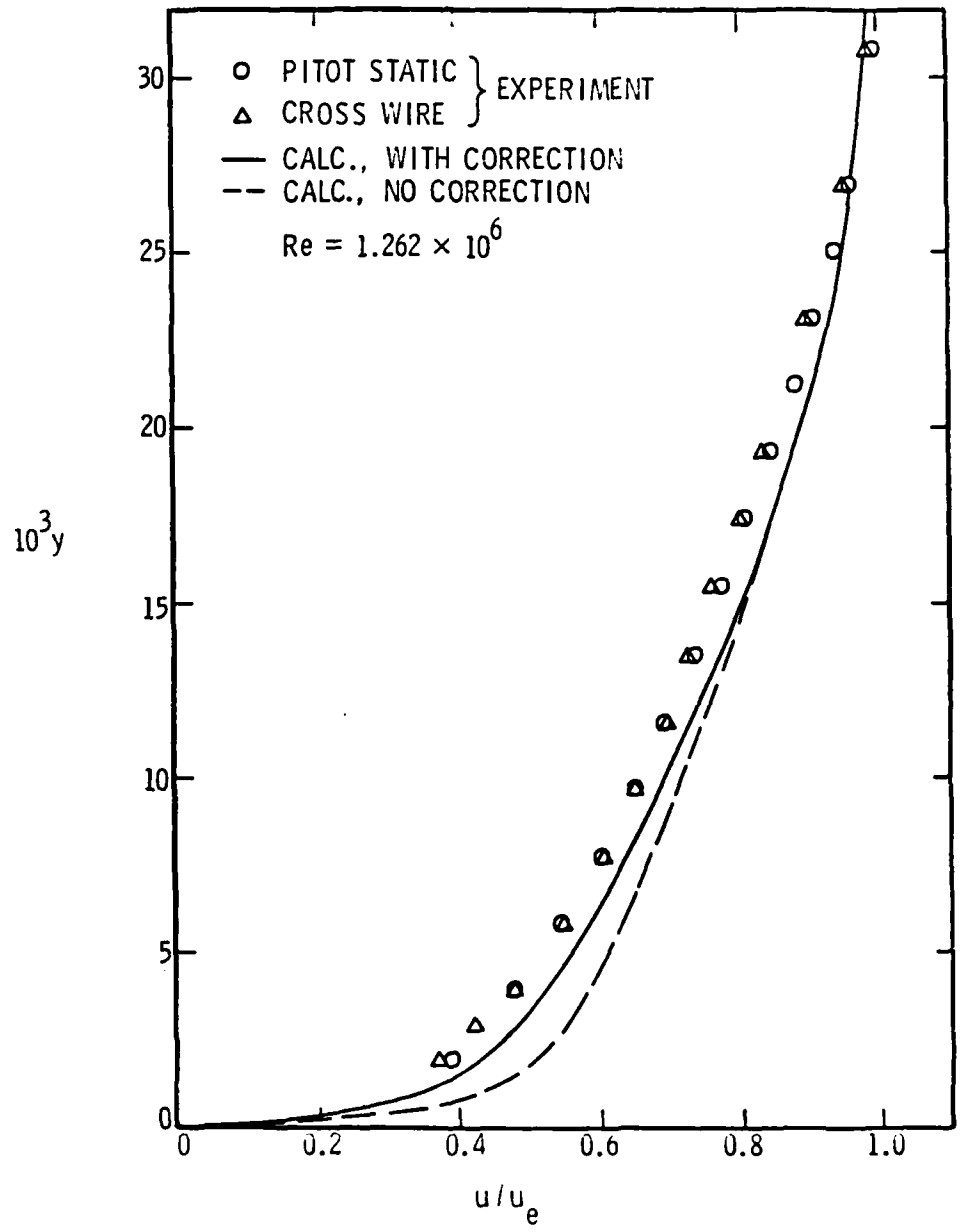

Figure 19. Mean Velocity Profile at x_o = 0.93, Modified Spheroid.

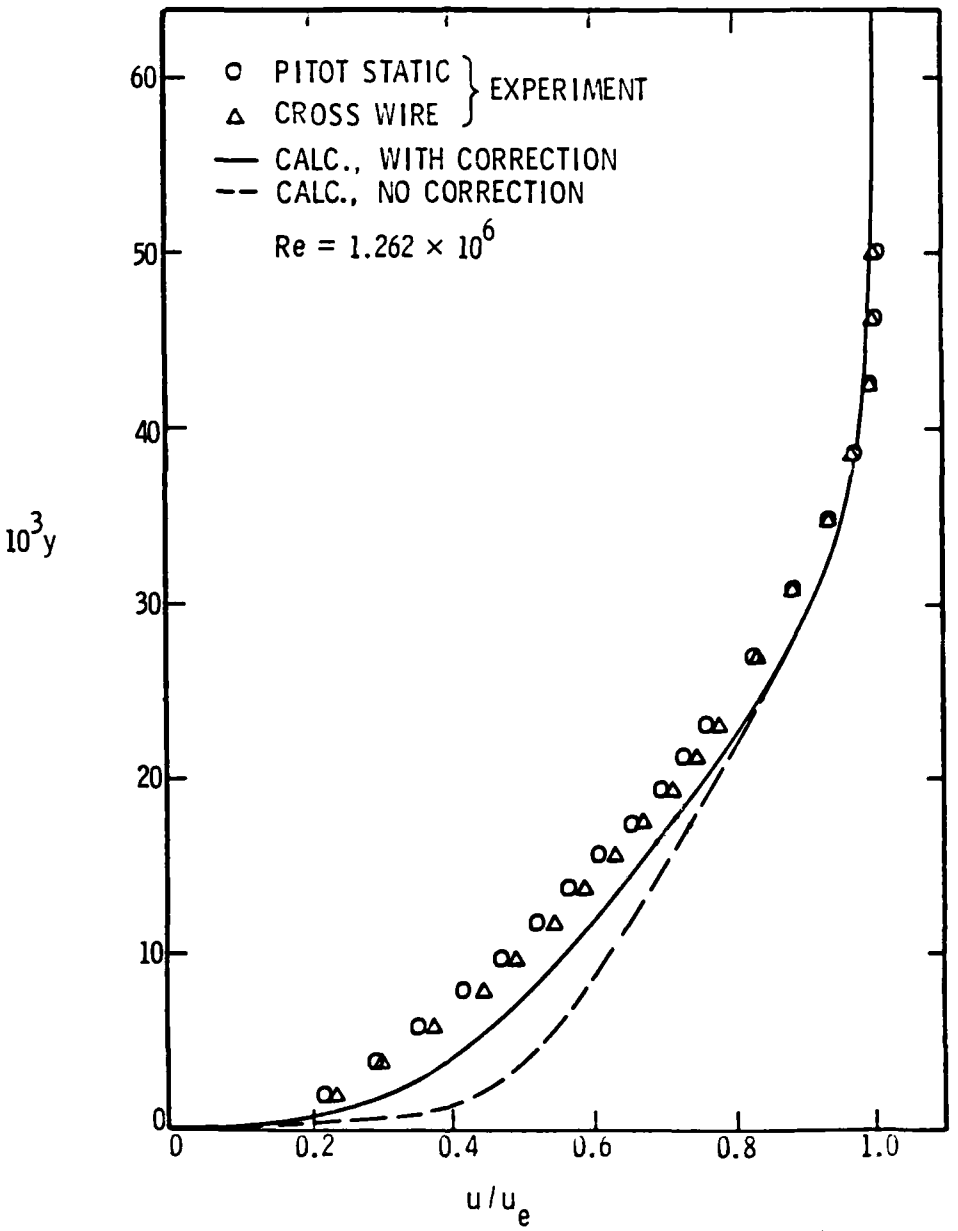

Figure 20. Mean Velocity Profile at x_o = 0.96, Modified Spheroid.

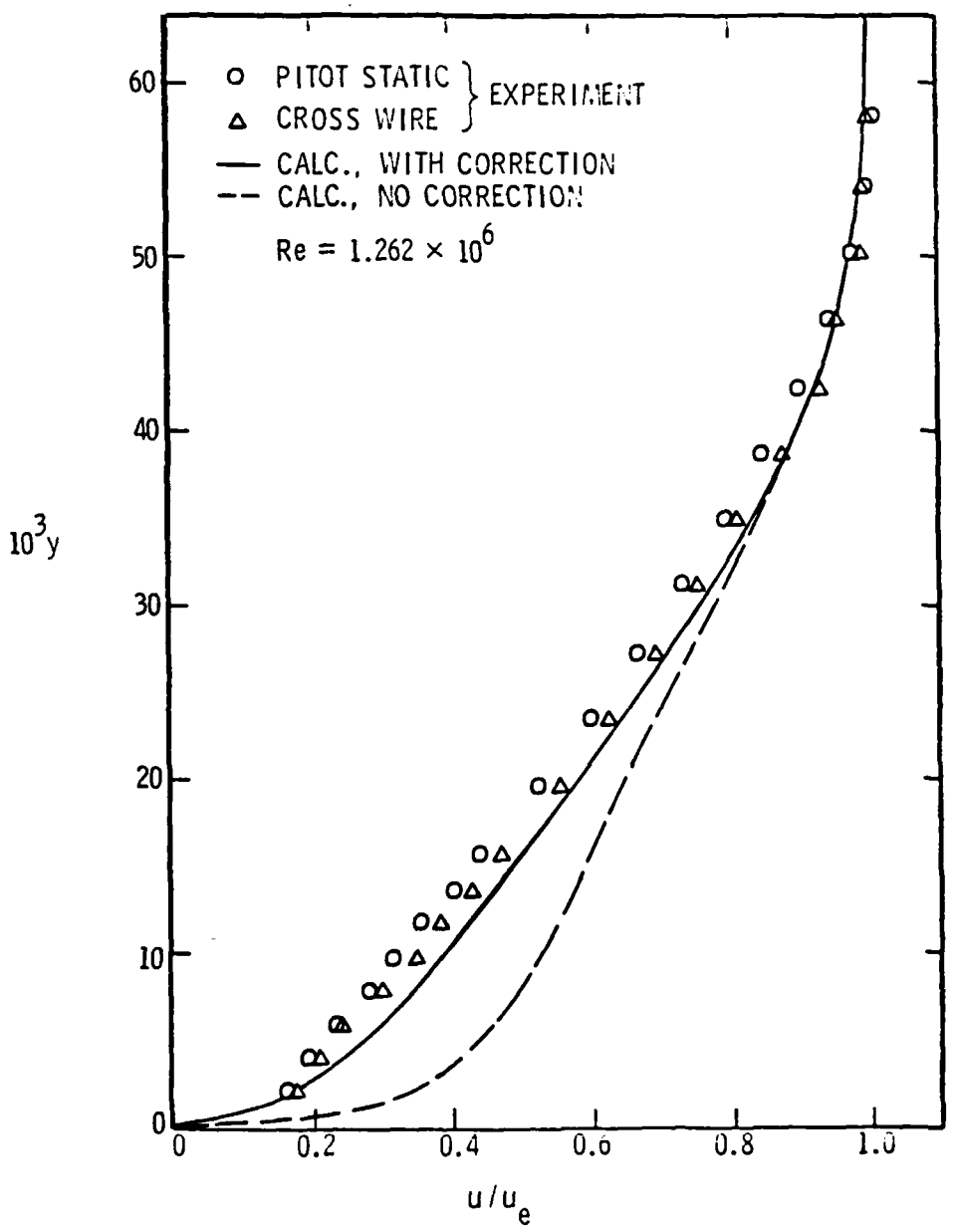

Figure 21. Mean Velocity Profile at x_o = 0.99, Modified Spheroid.

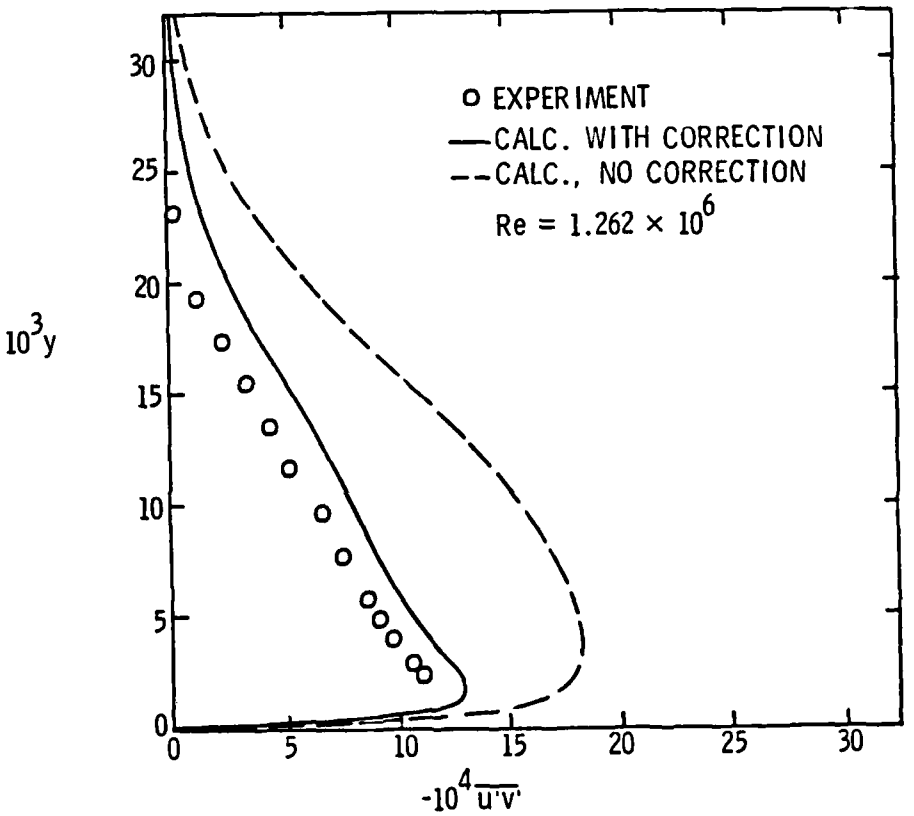

Figure 22. Reynolds Stress Profile at x_o = 0.90, Modified Spheroid.

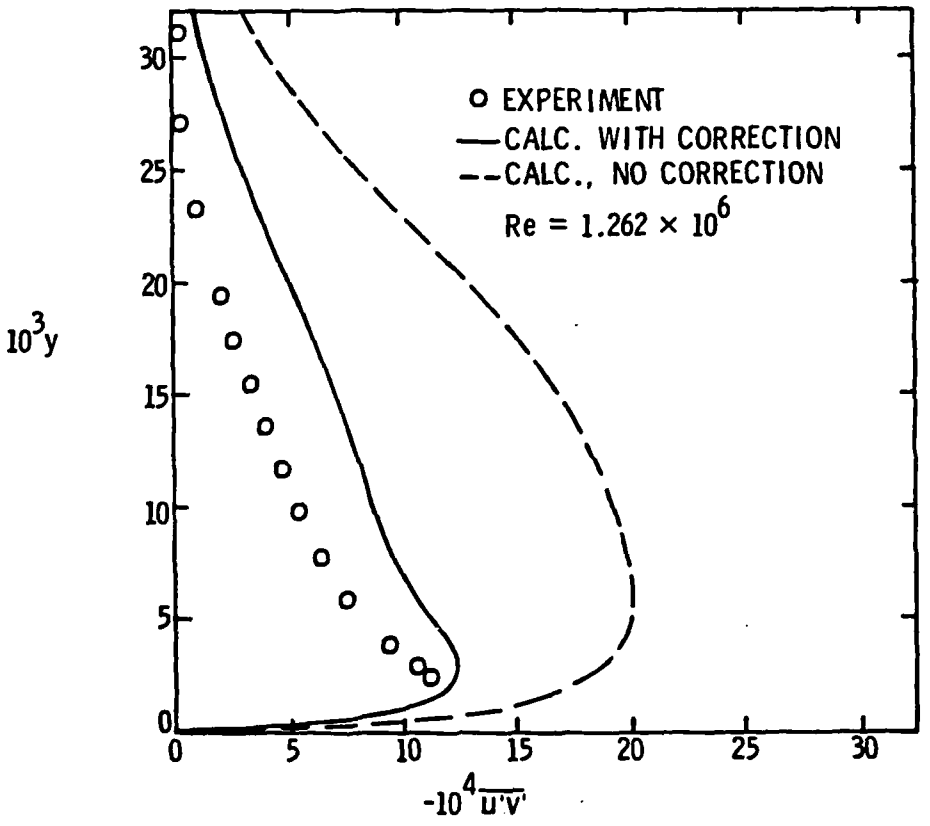

Figure 23. Reynolds Stress Profile at x_o = 0.93, Modified Spheroid.

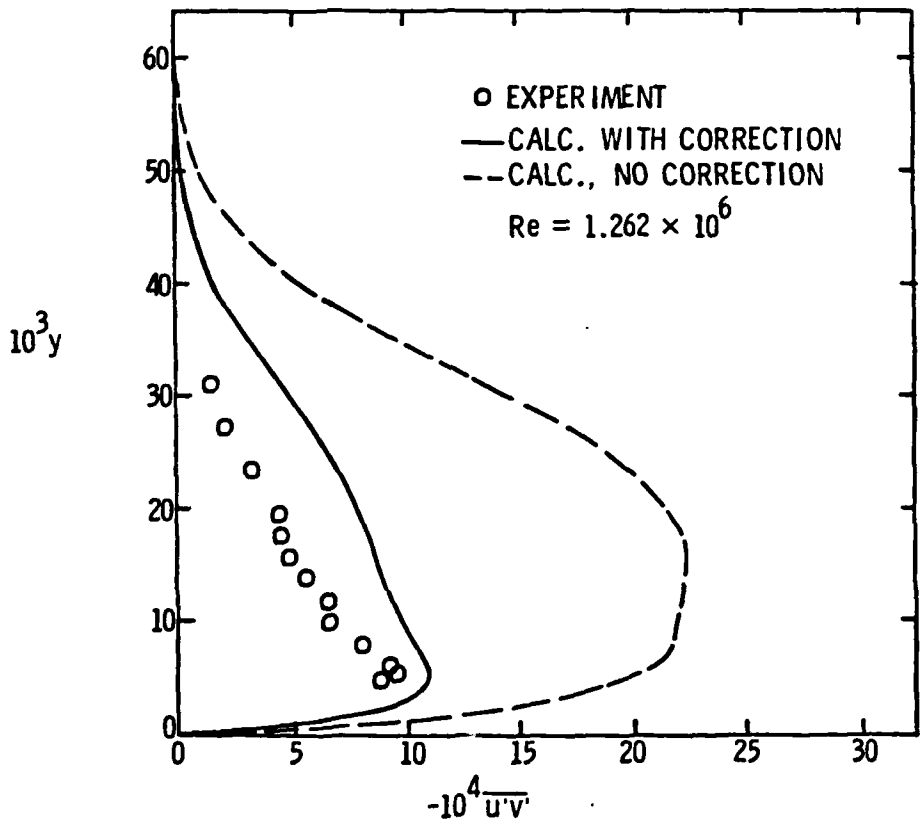

Figure 24. Reynolds Stress Profile at x_o = 0.96, Modified Spheroid.

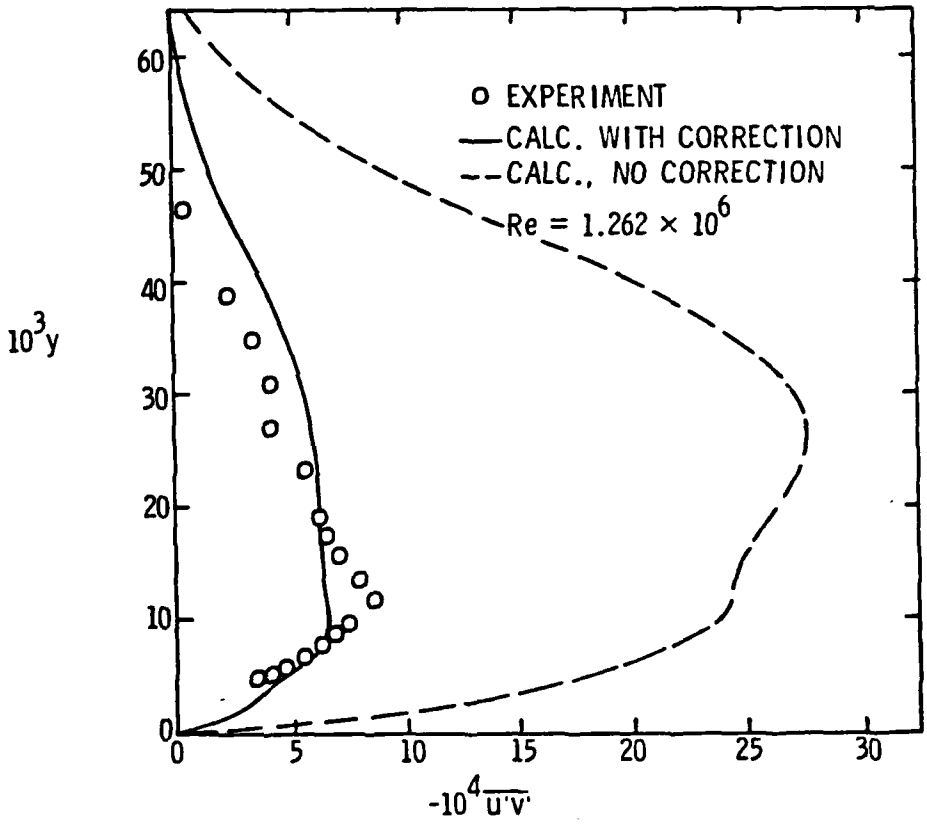

Figure 25. Reynolds Stress Profile at x_o = 0.99, Modified Spheroid.

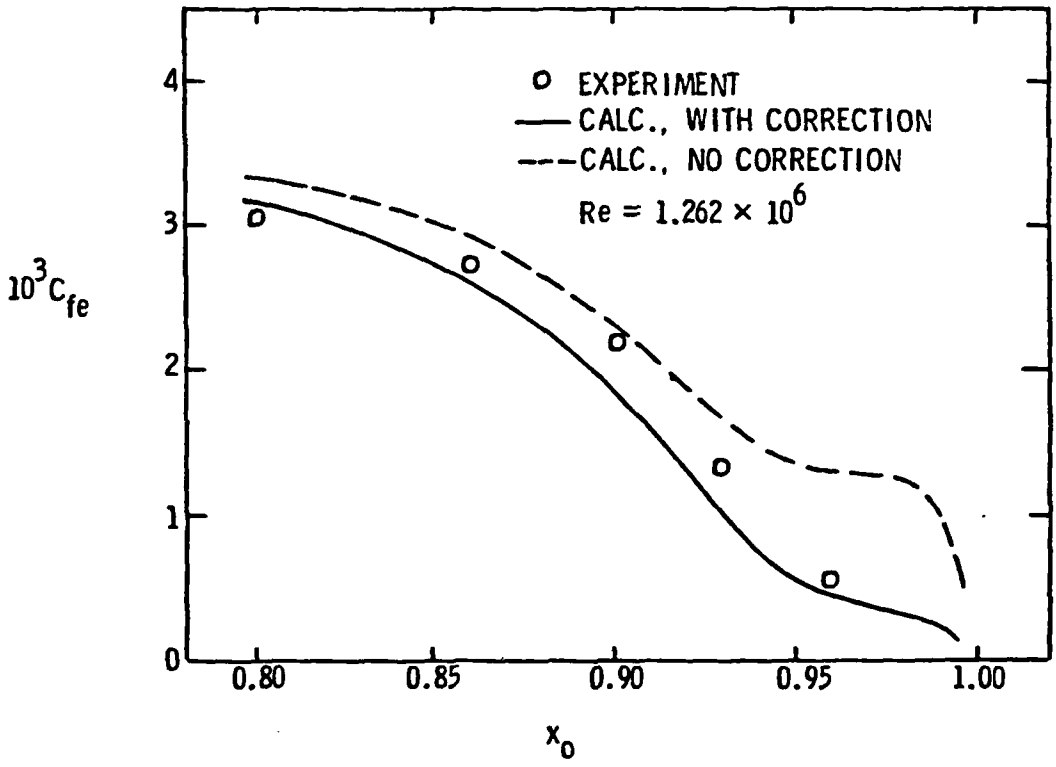

Figure 26. Skin Friction Coefficient Distribution, Modified Spheroid.

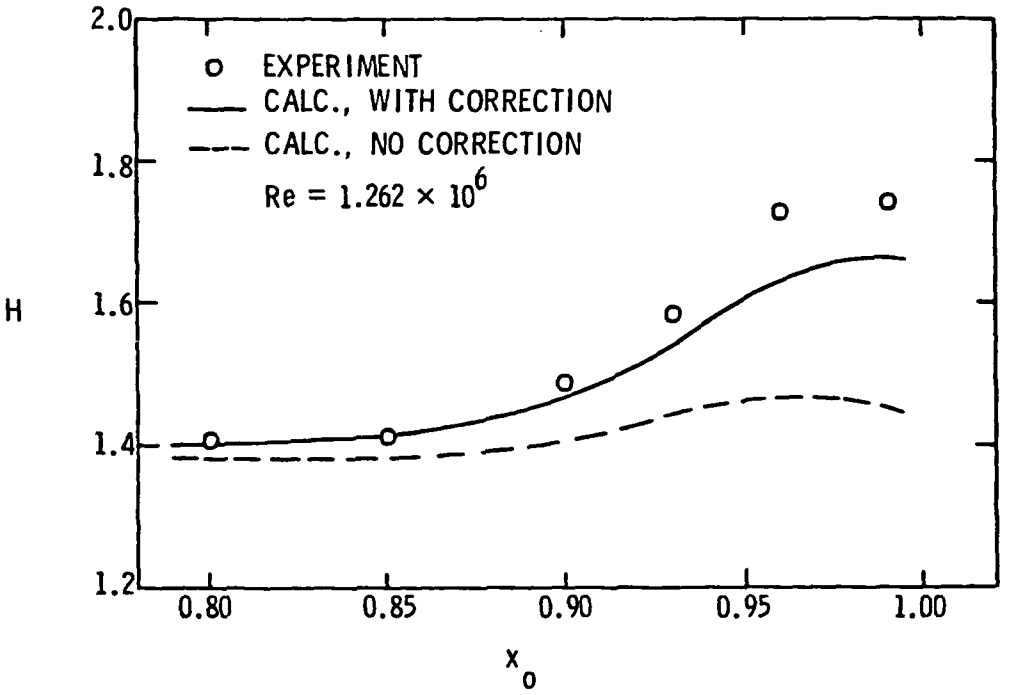

Figure 27. Shape Factor Distribution, Modified Spheroid.

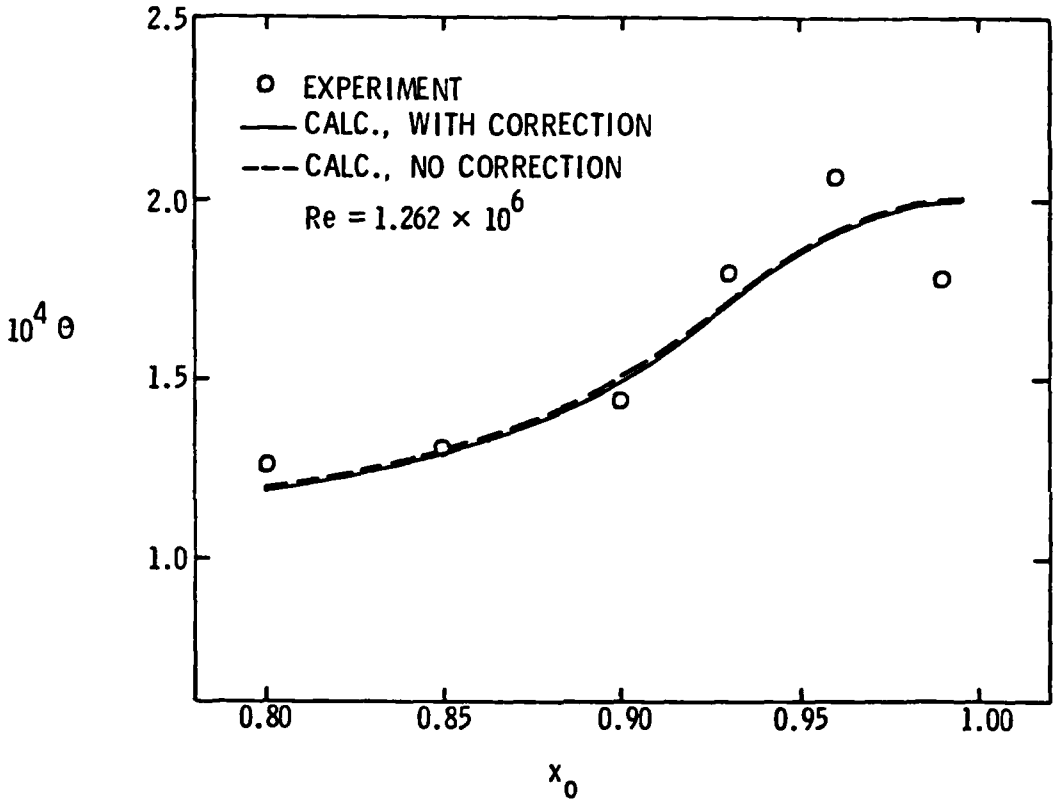

Figure 28. Momentum Deficit Area Distribution, Modified Spheroid.

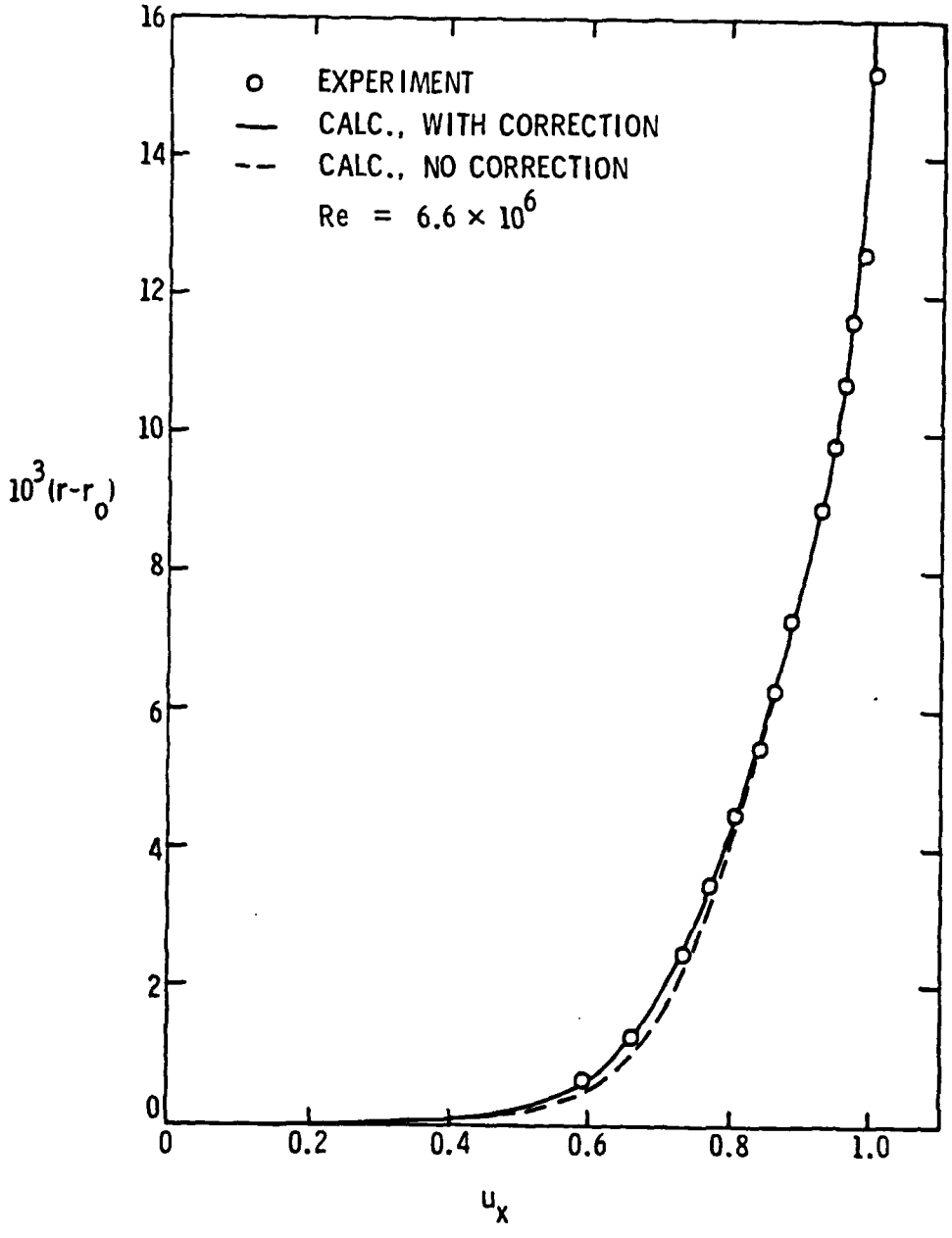

Figure 29. Mean Velocity Profile at x_o = 0.846, NSRDC Body.

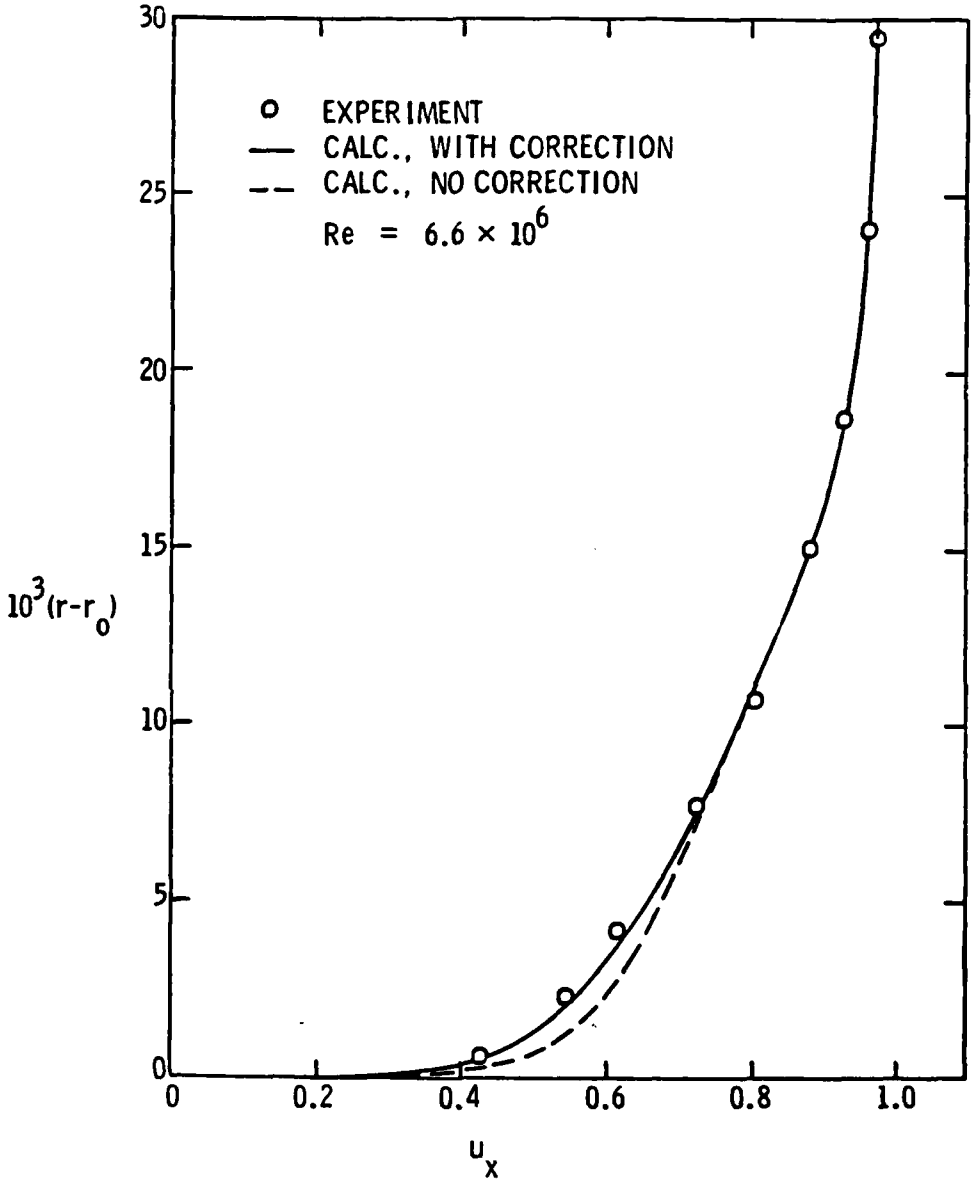

Figure 30. Mean Velocity Profile at x_o = 0.934, NSRDC Body.

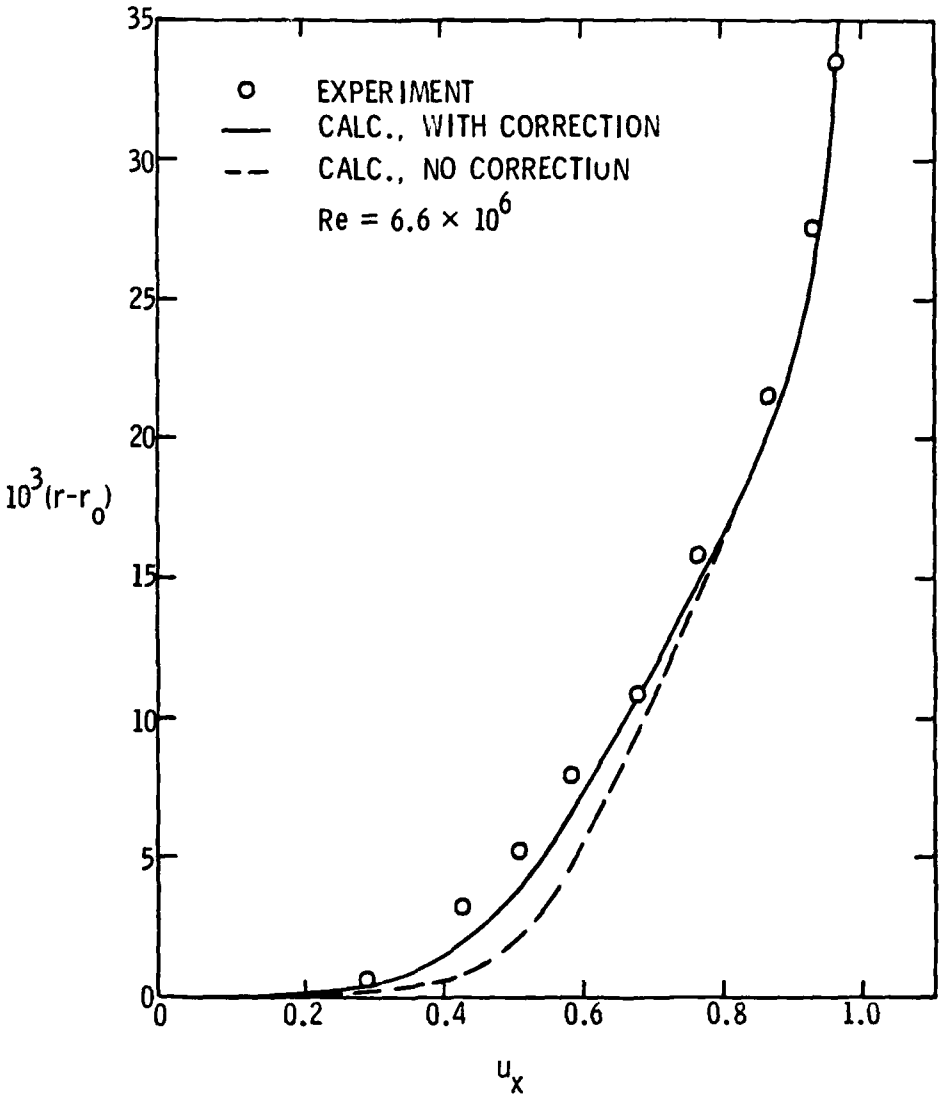

Figure 31. Mean Velocity Profile at x_o = 0.964, NSRDC Body.

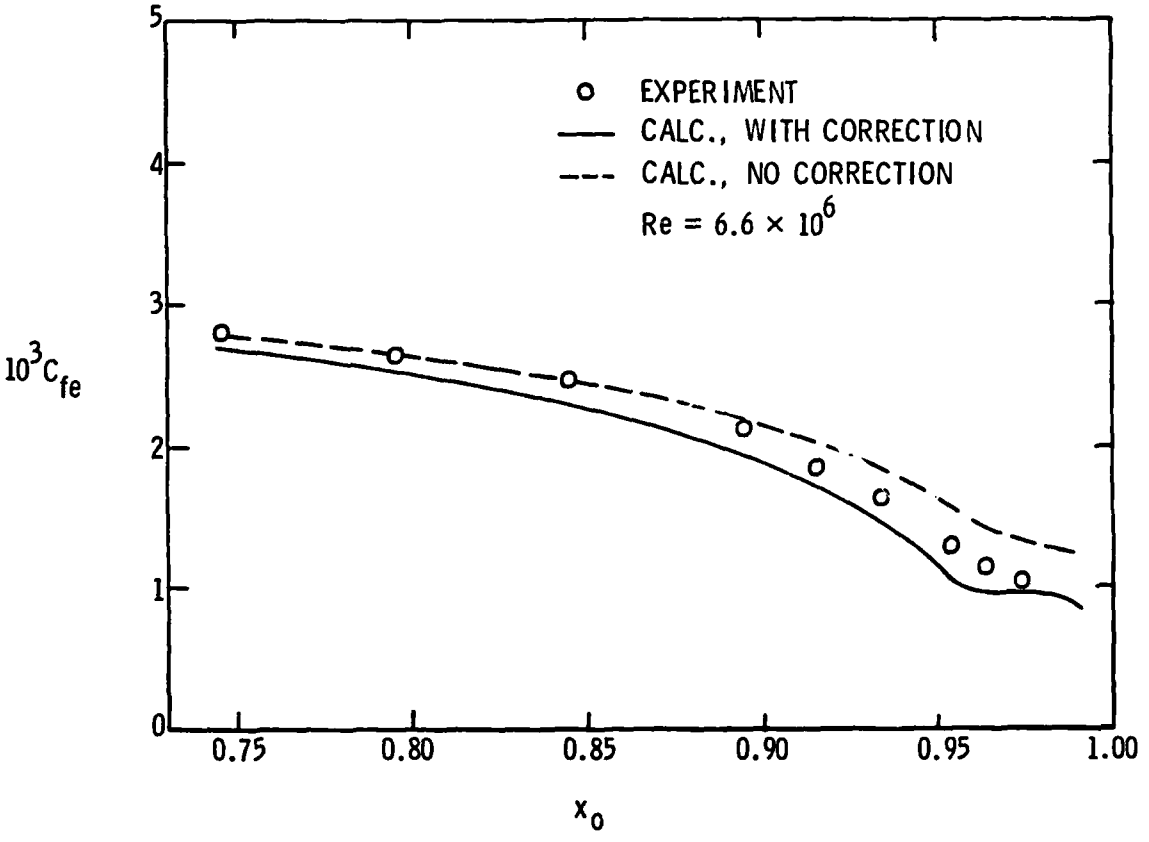

Figure 32. Skin Friction Coefficient Distribution, NSRDC Body.

DISTRIBUTION LIST FOR UNCLASSIFIED ARL TM 82-201 by G. H. Hoffman, dated 30 September 1982.

Commander
Naval Sea Systems Command
Department of the Navy
Washington, DC 20362
Attn: T. E. Peirce
Code NSEA-63R31
(Copy No. 1)

Commander
Naval Underwater Systems Center
Newport, RI 02840
Attn: D. Goodrich
Code 3634
(Copy No. 2)

Naval Underwater Systems Center
Attn: Q. Huynh
Code 3711
(Copy No. 3)

Commander
David W. Taylor Naval Ship R&D Center
Department of the Navy
Bethesda, MD 20084
Attn: T. T. Huang
Code 1552
(Copy No. 4)

Commander
Naval Surface Weapons Center
Silver Spring, MD 20910
Attn: W. J. Glowacki
Code R-44
(Copy No. 5)

Office of Naval Research
Department of the Navy
Arlington, VA 22217
Attn: H. Fitzpatrick
Code 438
(Copy No. 6)

Office of Naval Research
Attn: A. H. Gilmore
Code 220
(Copy No. 7)

Defense Technical Information Center
5010 Duke Street
Cameron Station
Alexandria, VA 22314
(Copy Nos. 8 through 13)

Naval Research Laboratory
Washington, DC 20390
Attn: Library
(Copy No. 14)

Superintendent
Code 1424
Naval Postgraduate School
Monterey, CA 93949
(Copy No. 15)

NASA Lewis Research Center
21000 Brookpark Road
Cleveland, OH 44135
Attn: J. Adamczyk
Chief, Computational
Fluid Mechanics Branch
(Copy No. 16)

Dr. James E. Carter, Manager
Computational Fluid Dynamics
United Technologies Research Center
East Hartford, CT 06108
(Copy No. 17)

Prof. V. C. Patel
Iowa Institute of Hydraulic Research
The University of Iowa
Iowa City, IA 52240
(Copy No. 18)

Professor C. L. Merkle
The Pennsylvania State University
Department of Mechanical Engineering
University Park, PA 16802
(Copy No. 19)

B. Lakshminarayana
The Pennsylvania State University
Department of Aerospace Engineering
University Park, PA 16802
(Copy No. 20)

The Pennsylvania State University
Applied Research Laboratory
Post Office Box 30
State College, PA 16801
Attn: R. E. Henderson
(Copy No. 21)

Applied Research Laboratory
Attn: S. A. Abdallah
(Copy No. 22)

DISTRIBUTION LIST FOR UNCLASSIFIED ARL TM 82-201 by G. H. Hoffman, dated 30 September 1982.

Applied Research Laboratory
Attn: G. C. Lauchle
(Copy No. 23)

Applied Research Laboratory
Attn: W. S. Gearhart
(Copy No. 24)

Applied Research Laboratory
Attn: G. H. Hoffman
(Copy No. 25)

Applied Research Laboratory
Attn: W. R. Hall
(Copy No. 26)

Applied Research Laboratory
Attn: J. J. Eisenhuth
(Copy No. 27)

Applied Research Laboratory
Attn: B. E. Robbins
(Copy No. 28)

Applied Research Laboratory
Attn: GTWT Files
(Copy No. 29)